Research Square

Preprints are preliminary reports that have not undergone peer review.
They should not be considered conclusive, used to inform clinical practice,
or referenced by the media as validated information.

WITHDRAWN: Interplay between cancer cells and M2 macrophages is necessary for miR-550a-3-5p down-regulation-mediated HPV-positive OSCC progression

Mingxin Cao
Sichuan University West China College of Stomatology
Weilong Zhang
Sichuan University West China College of Stomatology
Xianghua Yu
Sichuan University West China College of Stomatology
Jiashun Wu
Sichuan University West China College of Stomatology
Xinwei Qiao
Sichuan University West China College of Stomatology
Meichang Huang
Sichuan University West China College of Stomatology
Ke Wang
Sichuan University West China College of Stomatology
Jingbiao Wu
Sichuan University West China College of Stomatology
Yajie Tang
Shandong University
Jian Jiang
Sichuan Cancer Hospital and Research Institute
Xinhua Liang
Sichuan University West China College of Stomatology
Ya-ling Tang
tangyaling@scu.edu.cn

Research

Keywords: Human papillomavirus, OSCC, microRNA, EMT, microenvironment

Posted Date: April 23rd, 2020

DOI: https://doi.org/10.21203/rs.3.rs-23980/v1

License: This work is licensed under a Creative Commons Attribution 4.0 International License.
Read Full License

Version of Record: A version of this preprint was published at Journal of Experimental & Clinical Cancer Research on June 3rd, 2020. See the published version at https://doi.org/10.1186/s13046-020-01602-1.

EDITORIAL NOTE:

The full text of this preprint has been withdrawn by the authors while they make corrections to the work. Therefore, the authors do not wish this work to be cited as a reference. Questions should be directed to the corresponding author.

Abstract

Background: Human papillomavirus (HPV)-positive oral squamous cell carcinoma (OSCC) is increasing worldwide with typically higher grade and stage. Studies suggested that microRNAs (miRNAs) play a critical role in cancer; However, their role in HPV-positive OSCC progression remains unclear.

Methods: miRNA microarray was performed to identify differentially expressed miRNAs. qRT-PCR and FISH were performed to determine the relative expression of miR-550a-3-5p. CCK-8, Flow cytometry, Wound healing, Cell invasion assays and xenograft experiments were conducted to analyze the biological roles of miR-550a-3-5p. Tumor-associated macrophages (TAMs) generation, co-culturing of cancer cells with TAMs, Western blot, Dual-luciferase reporter gene assay, Immunohistochemistry and animal studies were performed to explore the mechanisms underlying the functions of miR-550a-3-5p.

Results: In this study, we identified 19 miRNAs differentially expressed in HPV-positive OSCC specimens. One of these, miR-550a-3-5p, was down-regulated in HPV-positive OSCC. This down-regulation correlated with higher tumor size and nodal metastasis. Biofunctional investigations revealed that miR-550a-3-5p inhibited tumor growth and progression in nude mice models without altering the in vitro migration, invasion and EMT of HPV-positive OSCC cells. After co-culturing cancer cells with tumor-associated macrophages (TAMs), we found that the effects of miR-550a-3-5p on suppressing migration, invasion and EMT of HPV-positive OSCC cells were dependent on decreasing M2 macrophages polarization. Moreover, we identified that miR-550a-3-5p, down-regulated by E6 oncoprotein, inhibited M2 macrophages polarization by YAP/CCL2 signaling, which in turn abrogating EMT program in HPV-positive OSCC cells. Using YAP inhibitor, verteporfin (VP) in a HPV-positive OSCC model of transgenic mice also showed that tumors were less progressive when compared to those in Vehicle group. In both xenografts and clinical HPV-positive OSCC samples, miR-550a-3-5p levels were inversely associated with YAP, CCL2 expressions and the number of M2 macrophages.

Conclusions: E6/miR-550a-3-5p/YAP/CCL2 signaling induces M2 macrophages polarization to enhance EMT and progression, revealing a novel crosstalk between cancer cells and immune cells in HPV-positive OSCC microenvironment.

Background

Oral squamous cell carcinoma (OSCC) ranks the sixth most common malignancies around the world, with a relatively lower five-year survival rate of approximate 50% (1). Traditionally, OSCC has been correlated with excessive tobacco and alcohol consumption. This view has recently been updated with epidemiological data showing that high-risk human papillomaviruses (HPVs), particularly HPV-16, have emerged as an additional causative agent of OSCC (2). HPV-positive OSCC defines a novel and independent entity with distinct genetic nature and clinicopathological features when compared to HPV-negative OSCC, while treatment approaches towards them are essentially the same which depend on the site and stage of the tumor (3). Even though patients with HPV-positive OSCC show better prognosis (4),

they are typically associated with positive lymph nodes, and current treatments still fail to cure more than a quarter of them with advanced stages (5–7). Therefore, there is an urgent need to study the molecular mechanisms responsible for invasive phenotype and progressive potentials in HPV-positive OSCC.

Migration and invasion of tumor cells into surrounding microvasculature of the lymphatic system, are crucial steps of the lymphatic dissemination of malignant tumors (8). During this process, the so-called epithelial-mesenchymal transition (EMT) is taken place with increased mesenchymal markers such as Vimentin and N-cadherin, and decreased epithelial markers such as E-cadherin and β-catenin (9). At present, emerging studies have showed that tumor-associated macrophages (TAMs), which are derived from peripheral blood monocytes and the most abundant among tumor-infiltrating immune cells, exert critical functions in tumor metastasis via modulating EMT (10). Stimulated by various secreted factors in tumor microenvironment, M1 or M2 macrophages can be polarized from TAMs. M1 macrophages exhibit pro-inflammatory roles and promote immune response to prevent oncogenic impacts, while M2 macrophages are important for pro-tumorigenic processes, and stimulation of tumor angiogenesis, cancer progression, immunosuppression, and matrix remodeling (11). In triple-negative breast cancer (TNBC), cancer cells-derived IL-6 could stimulate M2 macrophages polarization, which promoted EMT and invasiveness of TNBC cells (12). In addition, Li and colleagues have reported that hepatocellular carcinoma-conditioned TAMs possessed M2-like phenotype, and could contribute to the EMT and invasion in hepatocellular carcinoma (13). Conversely, in a study of breast cancer, not only TAMs could induce EMT, but mesenchymal-like cancer cells could in turn activate more macrophages recruitment by secreting GM-CSF and promote cancer metastasis (14). Although evidence has shown that HPV-positive OSCC exhibited enhanced immune activity with respect to HPV-negative OSCC (15), the crosstalk between the intrinsic mechanisms of cancer cells and the extrinsic microenvironmental factors such as TAMs that influences EMT and progression of HPV-positive OSCC remains unclear.

microRNAs (miRNAs) include a class of endogenous, noncoding small RNAs (19–24 nucleotides), which serve as post-transcriptional gene regulators to impact comprehensive biological processes (16). Multiple studies have uncovered that miRNAs have crucial roles in the development and progression of human cancers, exerting their effects by affecting the intrinsic mechanisms, or communicating with extrinsic properties (17, 18). However, while deregulated miRNAs have already been reported in HPV-positive OSCC (19, 20), the underlying mechanisms of whether miRNAs could orchestrate HPV-positive OSCC progression have remained limited. Hence, we speculated that miRNAs could mediate the crosstalk between cancer cells and TAMs to regulate malignant behaviors of HPV-positive OSCC.

In the present study, we clarified that decreased miR-550a-3-5p expression was correlated with HPV-positive OSCC metastasis. Functional experiments identified that miR-550a-3-5p inhibited M2 macrophages polarization, which in turn suppressed migration, invasion and EMT of HPV-positive OSCC cells. Furthermore, mechanistic studies revealed that miR-550a-3-5p, reduced by E6 oncoprotein, inhibited M2 macrophages polarization by regulating YAP/CCL2 axis, the correlation of which was confirmed in both xenografts of nude mice and clinical specimens. These findings improved our knowledge of the

molecular mechanisms by which miRNA regulated HPV-positive OSCC progression, and provided possible therapeutic target for HPV-positive OSCC.

Methods

Patients and clinical specimens

70 primary OSCC tissue specimens were collected from patients with informed consent at West China Hospital of Stomatology, Sichuan University. All of these patients have undergone the curative resection and were devoid of prior treatment or autoimmune diseases. Specimens were identified as squamous cell carcinoma and classified into different grades based on the current Union for International Cancer Control (UICC) criteria. Besides, 20 normal oral mucosa were obtained and all tissues samples were half frozen for RNA and DNA extraction, and half fixed in 10% formalin and embedded in paraffin. The current study was authorized by the Institutional Ethics Committee of the West China Medical Center, Sichuan University, China.

Hpv Detection

Total DNA was extracted using DNA Extraction Kit (Tiangen) according to manufacturer's instructions. HPV status was determined using a highly sensitive PCR protocol (Invitrogen) and HPV-16/18 primers, which was performed on a C1000 Touch PCR machine (Bio-Rad). Specific primers for HPV16: forward, 5'-CACAGTTATGCACAGAGCTGC-3', reverse, 5'-CATATATTCATGCAATGTAGGTGTA-3'; HPV-18: forward, 5'-CACTTCACTGCAAGACATAGA-3', reverse, 5'-GTTGTGAAATCGTCGTTTTTCA-3'. Then, eletrophoresis with 1.5% agarose gels was used to separate PCR products, which were visualized by GCLSTAIN staining.

Mirna Microarray

An Agilent miRNA microarray (8*60K, Design ID: 070156) using clinical specimens from HPV-positive and HPV-negative OSCC patients was carried out to profile miRNA by oeBiotech Limited Company. Total RNA was extracted using TRIzol reagent (Invitrogen) following manufacturer's protocols and 100 ng RNA per sample was used in microarray.

Qrt-pcr

Total RNA was extracted as previously defined. For mature miRNAs, All-in-One™ miRNA First-Strand cDNA Synthesis Kit (Genecopoeia) was used to generate 10 μL cDNA. Then using miR-specific primers and universal adaptor PCR primers (Genecopoeia), qRT-PCR was performed with All-in-One™ miRNA qRT-PCR Detection Kit (Genecopoeia) on CFX Connect Real-Time System (Bio-Rad). For mRNA, the reverse transcription was carried out using HiScript II Q RT SuperMix (Vazyme), and qRT-PCR was performed with

ChamQ™ SYBR Color qPCR Master Mix (Vazyme) on CFX Connect Real-Time System (Bio-Rad) (21). Specific primers for qRT-PCR of mRNA were listed in Supplementary Data. The U6 small nuclear RNA or GAPDH was used as an endogenous control. Each experiment was repeated at least three times and the results were analyzed using $2^{-\triangle\triangle CT}$ method.

Western Blot

The whole proteins were extracted using cell lysis buffer. Then, SDS-PAGE was used to separate proteins with different sizes. After that, gel was transferred to a PVDF membrane (Millipore) and target protein was immunoblotted with specific primary antibody. Primary antibodies were listed as follows: anti-E-cadherin (1:5000, mouse anti-human, Cell Signaling Technology Inc.), anti-Vimentin (1:2000, mouse anti-human, Abcam), anti-HPV16 E6 + HPV18 E6 (1:1000, mouse anti-human papillomavirus, Abcam), anti-HPV16 E7 (1:1000, mouse anti-human papillomavirus, Abcam), anti-YAP (1:2000, mouse anti-human, Proteintech), anti-TAZ (1:2000, mouse anti-human, Proteintech), anti-CCL2 (1:2000, mouse anti-human, Proteintech), anti-flag-YAP (1:1000, mouse, Abbkine), anti-GAPDH (1:2000, rabbit anti-human, Sigma-Aldrich). After incubating goat anti-rabbit or goat anti-mouse secondary antibody (MultiSciences), immunoblots were visualized using the chemiluminescence (ECL) reagent (Beyotime Biotechnology) and ChemiDoc XRS + System (Bio-Rad).

Mirna Fluorescence In Situ Hybridization (fish)

FISH assays were performed using miRNA Fluorescence In Situ Hybridization Kit (GenePharma) according to the instructions. Oligonucleotide modified probe labeled with cy3 for hsa-miR-550a-3-5p was provided by GenePharma. First, 5 μm formalin-fixed paraffin-embedded sections were preheated for 30 min at 60 ℃ and fresh xylene was used to remove paraffin from the tissue. Then, sections were rehydrated by 5 min incubations in decreasing concentrations of ethanol, and incubated with Proteinase K solution for 15 min at 37 ℃ and denaturing solution for 8 min at 78 ℃. After dehydration, probes were added in the hybridization solution and incubated for 4 h at 50 ℃. Sections were washed and counterstained with DAPI (GenePharma). Images were acquired using a fluorescence microscope (Olympus BX51).

Immunohistochemistry (ihc)

Formalin-fixed paraffin-embedded sections were firstly deparaffinized using xylene and rehydrated in alcohol with decreasing concentrations. Then boiling for 3 min in 0.01 M citrate buffer (pH = 6.0) was used for antigen retrieval, and 3% hydrogen peroxide was added for blocking endogenous peroxidase activity. After that, we used 5% goat serum for antigen blocking and incubated sections with the primary antibody at 4 ℃ overnight in a moist chamber. Sections were washed with PBS, and incubated first with biotinylated anti-mouse/rabbit IgG and sequent with streptavidin-biotin peroxidase both for 15 min. DAB

was added to detect the primary antibody, and hematoxylin was used to stain the nucleus. As negative controls, sections were analyzed in parallel except incubating with isotype-specific immunoglobulin (IgG) instead of the primary antibody. And the following primary antibodies were listed: anti-p16 (1:500, rabbit anti-human, Bioss), anti-Ki-67 (1:200, rabbit anti-human, HUABIO), anti-E-cadherin (1:500, mouse anti-human, Cell Signaling Technology Inc.), anti-Vimentin (1:200, mouse anti-human, Abcam), anti-CD31 (1:300, rabbit anti-human, Biorbyt), anti-CD34 (1:300, mouse anti-human, HUABIO), anti-YAP (1:600, mouse anti-human, Proteintech), anti-CCL2 (1:200, mouse anti-human, Proteintech), anti-CD163 (1:500, rabbit anti-human, Biorbyt). HE staining was referred to as hematoxylin and eosin staining. Staining of IHC was evaluated in ten randomly selected fields at 400X magnification. Quantification was evaluated by three independent investigators who were blinded to patient characteristics. IHC staining scores were calculated as staining intensity × percentage of positive cells. Staining intensity was assigned as: 0 (negative), 1 (weak), 2 (moderate), 3 (strong). Percentage of positive cells was defined as: 0 (no positive cells), 1 (10% positive cells), 2 (10–50% positive cells), 3 (50% positive cells). For CD163 staining, positive cells in each field were counted and expressed as the mean value (22).

Cell Culture And Reagents

HPV-positive human OSCC cell lines UPCI:SCC090 and UM-SCC-47, HPV-negative human OSCC cell lines Cal-27, SCC25, and HSC3, normal human oral keratinocytes (NOK), dysplasia human oral keratinocytes (DOK), and human monocyte cell line THP-1 were obtained from State Key Laboratory of Oral Disease, Sichuan University. UPCI:SCC090 and UM-SCC-47 were cultured in MEM (Gibco) containing 1X non-essential amino acids (Sigma-Aldrich), 1 mM sodium pyruvate (Sigma) and 10% fetal bovine serum (FBS, Gibco), Cal-27 and HSC3 were cultured in DMEM (Gibco) containing 10% FBS, SCC25 was cultured in DMEM/F12 (Gibco) containing 10% FBS, NOK and DOK were cultured in EpiLife (Gibco), and THP-1 was cultured in RPMI 1640 medium (Gibco) with 10% FBS. All of them were maintained at 37 ℃ in a humidified atmosphere with 5% CO_2. For macrophage generation, THP-1 cells were induced by 200 nM PMA (Sigma-Aldrich) for 24 h. Then OSCC cells whether transfected or not, were cultured with serum-free medium for 24 h and the supernatant was collected and centrifuged at 1000 x g for 20 min, known as the conditioned media (CM). We obtained tumor-associated macrophages (TAMs) by culturing PMA-induced THP-1 cells in CM of OSCC cells for 24 h. Morphology and polarization of TAMs were observed and detected. Co-cultivation of TAMs and OSCC cells was performed with the non-contact transwell system (pore size 0.4 μm, corning). TAMs seeded in the upper chamber communicated with corresponding OSCC cells in the lower chamber for 48 h, and OSCC cells were harvested for further analysis.

Verteporfin (VP, Selleck) was dissolved in DMSO and used in the culture medium at a final concentration of 10 μM for 24 h. Recombinant human CCL2 (Sino Biological) was added to CM at 500 ng/mL before inducing PMA-THP-1 cells.

Transfections

miR-550a-3-5p mimic or inhibitor were obtained from GenePharma Co. Ltd., China. Small-interfering RNAs (siRNAs) targeting E6, E7, and YAP were designed and synthesized also by GenePharma Co. Ltd., China. The plasmid pCDH-EF1-YAP-5SA (FLAG-tagged) and the empty Vector were kindly provided by Dr. Fanyuan Yu in West China School of Stomatology, Sichuan University and used for overexpression of activated YAP. These transfections were performed using EndoFectin™ (GeneCopoeia) according to the manufacturer's instructions. 48 h after transfection, further experiments could be carried out. Stably-transfected OSCC cells with miR-550a-3-5p overexpression were derived from the parental cells by a fluorescence microscope (Olympus BX51) detection and puromycin (Sigma-Aldrich) selection.

Cell Proliferation Assay And Flow Cytometry-based Apoptosis Analysis

CCK-8 assay was used to study cell proliferation. Cells were seeded in 96-well plates at the density of 1×10^3 (cells/well), and the absorbance at 450 nm was measured on 24, 48, 72, 96, 120 hours with 10 μL of CCK-8 solution. Proliferative comparison of mimic-transfected cells or inhibitor-transfected cells was calculated by normalization with respect to NC: % cells = (mimic or inhibitor – corresponding NC)/ corresponding NC × 100. Difference of OD Value on 120 h and OD Value on 24 h was used for calculation. Each assay was carried out in triplicate.

Flow cytometry using the Annexin V-FITC Apoptosis Detection Kit (Invitrogen) was used to measure cell apoptosis. Cells were seeded in 6-well plates and digested after 48 h. Then, 1X Binding Buffer was used to resuspend cells. We stained cells with 5 μL of Annexin V-FITC Conjugate and 5 μL of Propidium Iodide Solution and incubated them for 30 min. Stained cells were analyzed using a FACScalibur (Becton-Dickinson). For comparison, % apoptotic cells = (mimic or inhibitor – corresponding NC)/ corresponding NC × 100. Experiments were conducted in triplicate.

Wound Healing Assay And Cell Invasion Assay

Cells were cultured in 6-well plates and starved in serum-free medium for 24 h after arriving at 100% confluence. A pipette tip was used to scratch the cells and form the gap space. After washing out the dead cells, photomicrographs were taken immediately and at a timepoint of 24 h. Closed scratch areas were calculated by ImageJ software. Each experiment was conducted in triplicate.

24-well transwell plates (pore size 8 μm, Millipore) were used for conducting Cell invasion assays. The upper chamber was coated with Matrigel (BD Bioscience) before 5×10^4 cells being seeded in it. After 24 h of cell adherence, medium was changed into serum-free in upper chamber and complete medium was added to lower chamber. Then, cells which have invaded through the Matrigel after 24 h incubation were stained with 0.1% crystal violet and counted under a microscope. Five pre-selected fields (× 200) were observed and assays were conducted in triplicate.

Imaging Of Macrophage Morphology

Fluorescent staining was used for observation of macrophage morphology. Macrophages were washed with PBS for three times, and fixed with 4% paraformaldehyde for 20 min. Then, PBS containing 0.5% Triton X-100 was used to permeabilize the cells for 5 min. After incubating cells with FITC-phalloidin (Solarbio) for 30 min, nuclei were stained using DAPI (Sigma-Aldrich). All photographs were taken using a fluorescence microscope (Olympus BX51).

Dual Luciferase Reporter Gene Assays

The wild-type or mutant YAP 3'UTR pEZX-FR02 plasmids designed by GeneCopoeia Co. Ltd., was cotransfected with miR-550a-3-5p mimic or NC in UPCI:SCC090 and UM-SCC-47 cells using EndoFectin™ (GeneCopoeia). 48 h after transfection, cell lysates were collected and used for detection of firefly and *Renilla* luciferase activities following the protocol of a Luc-Pair™ Duo-Luciferase Assay Kit 2.0 (GeneCopoeia). *Renilla* luciferase activity was used for normalization in the study.

Animal Experiments

All animal experiments were approved by the Institutional Animal Care and Use Committee of West China Medical Center, Sichuan University. For subcutaneous xenograft model of nude mice, twenty 4-week-old BALB/c male nude mice (Dashuo) were divided into four groups after 1 week acclimation. Stably miR-550a-3-5p-overexpressed UPCI:SCC090 and Cal-27 cells and their relevant empty vector-transfected control cells were injected into the right flank region of nude mice subcutaneously. 0.2 mL containing 5×10^6 cells per aliquot was used in each mouse. Tumor volumes were evaluated every three days and calculated using formula as below: length × $(\text{width})^2 \times \prod/6$. Mice were killed using isoflurane after 8 times taking notes of tumor volume, and tumors were collected for weights measuring and further examination.

For 4NQO-indued OSCC model of transgenic mice, a total of sixteen 7-week-old female Rosa26-E6-E7 constitutive knock-in C57BL/6 mice (Cyagen, ID: TOS150814BA1) were used and divided into two groups randomly after one week of acclimation: 4NQO + VP group (n = 8) and 4NQO group (n = 8). A solution of 4NQO (Sigma-Aldrich) was added to the distilled drinking water at a concentration of 100 μg/mL for 8 weeks, and then switched to distilled water for another 8 weeks to generate OSCC as we previously described (23). After that, VP (Selleck) was injected every three days intraperitoneally at 100 mg/kg in 4NQO + VP group, while Vehicle-treated mice were injected with DMSO. Mice were anesthetized using isoflurane after 6 doses of VP, and tongue was collected, carefully observated and longitudinally bisected. We fixed one part of each tongue tissue with 10% formalin and embedded it with paraffin, and froze the other part immediately and stored it at -80 ℃.

Statistical analysis

The correlations between miR-550a-3-5p expression and other clinicopathlogical factors were estimated using Chi-square analysis. Means comparisons were conducted with Student t-test or one-way ANOVA. The associations between miR-550a-3-5p and YAP, YAP and CCL2, and CCL2 and CD163 expressions in HPV-positive OSCC specimens were assessed using 2-tailed Pearson's statistics. All cellular experiments were conducted independently for at least three times and in triplicate each time. GraphPad Prism 7.0 (GraphPad Software) was used for processing all data and values were presented as means ± SD. P 0.05 was considered to be statistically significant.

Results

Down-regulation of miR-550a-3-5p correlated with HPV-positive OSCC metastasis

A total of 70 clinical specimens of OSCC were detected for HPV status using PCR analysis of extracted DNA (Supplementary Fig. 1A), and were grouped into HPV-positive OSCC (n = 25) and HPV-negative OSCC (n = 45). To identity the differentially expressed miRNAs between HPV-positive and HPV-negative OSCC, an Agilent human miRNA microarray was performed. As shown in Fig. 1A and Supplementary Table 1, 8 miRNAs were significantly up-regulated in HPV-positive OSCC samples, whereas the levels of 11 miRNAs were down-regulated compared with HPV-negative OSCC samples (Fold change ≥ 2, P 0.05). By in silico and literature analysis, we selected miR-550a-3-5p, miR-451a, and miR-210-3p to validate their expression differences. qRT-PCR showed that miR-550a-3-5p was down-regulated 10.3-fold in HPV-positive OSCC (n = 25) compared to HPV-negative OSCC tissue samples (n = 45, P 0.001) and 24.6-fold compared to normal (HPV-negative non-cancerous) tissue samples (n = 20, P 0.001), miR-451a was down-regulated 2.6-fold in HPV-positive OSCC compared to HPV-negative OSCC tissue samples (P = 0.002) and 4.2-fold compared to normal tissue samples (P 0.001), and miR-210-3p was up-regulated 1.5-fold in HPV-positive OSCC compared to HPV-negative OSCC tissue samples (P 0.001) and 2.1-fold compared to normal tissue samples (P 0.001) (Fig. 1B), which were all consistent with the microarray results. Ranked as the most differentially-expressed miRNAs, we therefore firstly concentrated on miR-550a-3-5p for further studies.

We verified miR-550a-3-5p expression levels and localization by utilizing miRNA fluorescence in situ hybridization (FISH). HPV infection was shown by immunohistochemistry staining of p16. The red fluorescent distribution indicated that miR-550a-3-5p was mainly localized in the cytoplasm of both OSCC and normal cells, and had a highest expression in normal mucosa while lowest expression in HPV-positive OSCC specimens (Fig. 1C). Additionally, miR-550 was also reported to be down-regulated in p16-positive oropharyngeal squamous cell carcinoma (OPSCC) compared to p16-negative OPC samples from other miRNA microarray data (Supplementary Fig. 1B) (20). Then, the qRT-PCR results of miR-550a-3-5p and their associations with corresponding clinicopathological features in HPV-positive and HPV-negtive OSCC patients were summarized. After differentiating miR-550a-3-5p expressions into lower and higher

part according to the cut-off point of their median, we found that in HPV-positive OSCC patients, lower miR-550a-3-5p expression was associated with higher tumor size ($P = 0.025$) and the presence of nodal metastasis ($P = 0.009$), but has no correlations with age, gender, drink, smoke, differentiation, clinical stage and recurrence (Table 1). However, miR-550a-3-5p expression was associated with none of these features in HPV-negative OSCC patients. Thus, miR-550a-3-5p levels were frequently down-regulated in HPV-positive OSCC, particularly in patients with higher tumor size and nodal metastasis, which indicated a potential role for miR-550a-3-5p in targeting HPV-positive OSCC progression.

Table 1
Clinicopathological features of HPV + ve/-ve OSCC patients and their relationship with miR-550a-3-5p expression

Characteristics	HPV + ve OSCC (n = 25)			HPV-ve OSCC (n = 45)		
	Cases	Low miR-550a-3-5p (%)	P	Cases	Low miR-550a-3-5p (%)	P
Age (years)						
< 60	20	10 (50.00)	0.689	21	9 (42.86)	0.300
≥ 60	5	3 (60.00)		24	14 (58.33)	
Gender						
Female	13	8 (61.54)	0.320	17	6 (35.29)	0.098
Male	12	5 (41.67)		28	17 (60.71)	
Drink						
Yes	7	4 (57.14)	0.748	31	15 (48.39)	0.587
No	18	9 (50.00)		14	8 (57.14)	
Smoke						
Yes	5	3 (60.00)	0.689	28	14 (50.00)	0.848
No	20	10 (50.00)		17	9 (52.94)	
Tumor Size						
T1-T2	9	2 (22.22)	**0.025***	20	8 (40.00)	0.182
T3-T4	16	11 (68.75)		25	15 (60.00)	
Differentiation						
Well	4	2 (50.00)	0.265	14	6 (42.86)	0.438
Moderate	13	5 (38.46)		19	9 (47.37)	
Poor	8	6 (75.00)		12	8 (66.67)	
Clinical stage						
-	14	5 (35.71)	0.066	17	8 (47.06)	0.672
-	11	8 (72.73)		28	15 (53.57)	
Nodal metastasis						
Yes	20	13 (65.00)	**0.009***	26	13 (50.00)	0.862

* $P < 0.05$ was regarded as statistically significant in Chi square test.

Characteristics	HPV + ve OSCC (n = 25)			HPV-ve OSCC (n = 45)		
	Cases	Low miR-550a-3-5p (%)	P	Cases	Low miR-550a-3-5p (%)	P
No	5	0 (0)		19	10 (52.63)	
Recurrence						
Yes	1	1 (100.00)	0.327	8	5 (62.50)	0.477
No	24	12 (50.00)		37	18 (48.65)	

* $P < 0.05$ was regarded as statistically significant in Chi square test.

miR-550a-3-5p inhibited tumor growth and progression in nude mice models without altering the in vitro migration, invasion and EMT in HPV-positive OSCC cells

To better investigate the biological behavior of miR-550a-3-5p in HPV-related OSCC, we transfected miR-550a-3-5p mimic and inhibitor into OSCC cell lines which express different endogenous miR-550a-3-5p levels. The same as expressional differences in tissue specimens, miR-550a-3-5p levels were highest in normal oral keratinocytes (NOK), then dysplasia oral keratinocytes (DOK), HPV-negative OSCC cell lines, and lowest in HPV-positive OSCC cell lines (Supplementary Fig. 1C). Up-regulation and down-regulation of miR-550a-3-5p in HPV-positive cell lines UPCI:SCC090 and UM-SCC-47, HPV-negative cell lines Cal-27 and SCC25 were confirmed by qRT-PCR (Supplementary Fig. 1D). miR-550a-3-5p overexpression decreased cell proliferation rate in HPV-positive (-25.01%, UPCI:SCC090; -40.08%, UM-SCC-47) and HPV-negative cells (-36.69%, Cal-27; -13.13%, SCC25), while its inhibition increased cell proliferation rate in HPV-positive (15.56%, UPCI:SCC090; 54.49%, UM-SCC-47) and HPV-negative cells (36.03%, Cal-27; 31.97%, SCC25) (Fig. 2A, Supplementary Fig. 2A). Using Flow cytometry assay, miR-550a-3-5p overexpression led to significantly increased apoptosis in case of HPV-positive (62.39%, UPCI:SCC090; 81.82%, UM-SCC-47) and HPV-negative cells (95.21%, Cal-27; 76.27%, SCC25), and inhibition decreased cell apoptosis (-45.55%, UPCI:SCC090; -62.63%, UM-SCC-47; -55.43%, Cal-27; -45.9%, SCC25) (Fig. 2B, Supplementary Fig. 2B). Furthermore, we performed Wound healing and Transwell invasion assays to detect the abilities of migration and invasion in miR-550a-3-5p-transfected HPV-positive and HPV-negative OSCC cells. The results showed that miR-550a-3-5p overexpression decreased the migrated area (14.64%, Cal-27; 11.04%, SCC25) and invasive ability (68.29%, Cal-27; 58.88%, SCC25) in HPV-negative cells, while had no evident impacts on HPV-positive cells. In contrast, miR-550a-3-5p inhibition increased the migrated area (22.68%, Cal-27; 10.34%, SCC25) and invasive ability (58.60%, Cal-27; 106.33%, SCC25) in HPV-negative cells, but still did not affect those in HPV-positive cells (Fig. 2C, D). As EMT leads a crucial role in the process of epithelial cancer progression (24), we examined both the epithelial and mesenchymal markers in miR-550a-3-5p-overexpressed HPV-positive and negative OSCC cells by qRT-

PCR. As can be seen in Fig. 2E, miR-550a-3-5p overexpression resulted in a significant increase in E-cadherin and decrease in Vimentin in HPV-negative cells, while had no effects on EMT of HPV-positive cells.

After in vitro studies, we stably transfected HPV-positive OSCC cells UPCI:SCC090 and HPV-negative OSCC cells Cal-27 with an miR-550a-3-5p lentiviral vector, which was confirmed by qRT-PCR (Supplementary Fig. 1E), and injected them into nude mice subcutaneously to establish the xenograft model. miR-550a-3-5p overexpression, both in HPV-positive and HPV-negative OSCC cells, led to a decrease in tumor volume and tumor weight with respect to the vector control group (Fig. 3A-C). HE staining and fluorescence in situ hybridization of miR-550a-3-5p were carried out to verify the xenografts (Supplementary Fig. 1F). Then, immunohistochemistry staining was used to analyze the expression of proliferative indicator Ki-67, EMT markers E-cadherin and Vimentin, and angiogenesis-related markers CD31 and CD34. Interestingly, Ki-67 and Vimentin were reduced but E-cadherin was increased, along with inhibited angiogenesis (CD31 and CD34) in both miR-550a-3-5p-overexpressed HPV-positive and HPV-negative OSCC cells-derived xenografts (Fig. 3D).

miR-550a-3-5p inhibited M2 macrophages polarization to suppress the migration, invasion, and EMT of HPV-positive OSCC cells

The above contradiction of in vitro and in vivo results in HPV-positive OSCC suggested that miR-550a-3-5p might participate in a cell nonautonomous mechanism to exert its tumor-suppressive effects. One possibility for miRNA to execute this function is to mediate the crosstalk between cancer cells and inflammatory cells, especially TAMs, which exhibit one of the most abundant types in tumor microenvironment (25). Thus, we utilized a model of TAMs to investigate whether there were underlying interactions (Fig. 4A). The human monocyte cell line THP-1 was incubated with PMA for 24 h and differentiated into macrophages, which then turned into TAMs after being cultured with conditioned media (CM) from HPV-positive OSCC cell lines (UPCI:SCC090 or UM-SCC-47). Morphologically, TAMs were stretched and elongated compared with PMA-induced THP-1 cells (Fig. 4B). Consistent with the observation above, M1 and M2 markers were both increased in OSCC cells-primed macrophages in contrast with that of PMA-induced THP-1 cells using qRT-PCR. However, Macrophages treated with CM from miR-550a-3-5p mimic-transfected HPV-positive cells exhibited lower levels of M2 macrophage markers including CD163, IL-10 and Arginase-1 when compared with those treated with CM from mimic NC-transfected HPV-positive cells, while M1 macrophage markers such as CD80, IL-12p40 and TNF-α showed no evident differences (Fig. 4C). These indicated that TAMs of a mixed M1/M2 phenotype were induced by HPV-positive OSCC cells, while miR-550a-3-5p overexpression down-regulated the polarization of M2 macrophages.

To investigate whether miR-550a-3-5p could suppress migration, invasion and EMT of HPV-positive OSCC cells by inhibiting M2 macrophages polarization, Wound healing and Transwell invasion assays were

performed in miR-550a-3-5p-overexpressed HPV-positive cells after being co-cultured with corresponding TAMs for 48 h. As shown in Fig. 4D, miR-550a-3-5p overexpression decreased the migrated area (14.10%, UPCI:SCC090; 23.12%, UM-SCC-47) and invasive ability (68.74%, UPCI:SCC090; 62.39%, UM-SCC-47) in HPV-positive cells. Meanwhile, we verified whether TAMs could suppress the EMT of miR-550a-3-5p-overexpressed HPV-positive cells. qRT-PCR showed that TAMs co-culture significantly increased the epithelial markers such as E-cadherin and β-catenin, and decreased the mesenchymal markers such as N-cadherin and Vimentin in miR-550a-3-5p-overexpressed HPV-positive cells. Up-regulated E-cadherin and down-regulated Vimentin protein levels were also detected in miR-550a-3-5p-overexpressed HPV-positive cells by Western blot (Fig. 4E). Taken together, our findings revealed that miR-550a-3-5p suppressed migration, invasion and EMT of HPV-positive OSCC cells by inhibiting M2 polarization.

miR-550a-3-5p, down-regulated by oncoprotein E6, directly targeted YAP in HPV-positive OSCC cells

We hypothesized that a mechanism between HPV-positive OSCC cells and TAMs exists that explains at least partly the previously depicted tumor-suppressive behaviors of miR-550a-3-5p. HPV virus expresses two main oncogenic proteins, E6 and E7 that target host tumor suppressor proteins to promote tumorigenesis and progression (26). We found that miR-550a-3-5p expression was induced after E6 knockdown, while not influenced after E7 inhibiting in HPV-positive cells (Fig. 5A, Supplementary Fig. 3A). This suggested that miR-550a-3-5p was down-regulated by E6 oncoprotein in HPV-positive OSCC cells. To determine what downstream signals of miR-550a-3-5p contributed to inhibitions of M2 macrophages polarization, we looked at the GO (molecular function) and KEGG (signaling pathway) analysis of miR-550a-3-5p. Results found that miR-550a-3-5p was related to the cytokine, chemokine activity, and Hippo signaling pathway (Supplementary Fig. 3D). As recent studies demonstrated critical functions of Hippo signaling in cancer immunity (27), we firstly detected expressions of its central transcription factors, YAP and TAZ. Overexpression of miR-550a-3-5p significantly inhibited YAP mRNA and protein levels in HPV-positive cells, but had no effects on TAZ expression (Fig. 5B). Then in silico analysis revealed that miR-550a-3-5p had three putative targets in 3’UTR of YAP mRNA, which were further validated by Dual luciferase reporter gene assays. As shown in Fig. 5C, Luc-YAP-3’UTR (wild type, WT) cotransfected with miR-550a-3-5p mimics in UPCI:SCC090 and UM-SCC-47 cells showed an obvious decrease of luciferase activity, while Luc-YAP-3’UTR (mutant, MUT) group had a minimal effect on that.

YAP/CCL2 was required for miR-550a-3-5p deficiency-mediated M2 macrophages polarization and M2 macrophages-induced EMT

Our results revealed that YAP was directly regulated by miR-550a-3-5p. Next, we performed qRT-PCR to assess several critical factors which have been reported to be regulated by YAP and affect cancer

immunity (28–31). Results found that CCL2 and CXCL5 were significantly inhibited after YAP knockdown in both UPCI:SCC090 and UM-SCC-47 cells, while TLR9 and CSF1 were not changed evidently in both of them. Moreover, only CCL2 expression showed an obvious decrease in miR-550a-3-5p-overexpressed UPCI:SCC090 and UM-SCC-47 cells, which led us to speculate that CCL2 may serve as a downstream factor of miR-550a-3-5p/YAP in HPV-positive OSCC (Fig. 5D, Supplementary Fig. 3B). As YAP regulates gene expression largely through binding to TEAD family transcription factors, we utilized a small molecule called verteporfin (VP) which could inhibit YAP-TEAD association to investigate whether CCL2 was regulated by YAP-TEAD complex (32). Results showed that mRNA and protein levels of CCL2 were significantly decreased upon VP treatment, clarifying the role of YAP-TEAD transcription activity in mediating CCL2 expression (Fig. 5E). To further analyze whether CCL2 was regulated by miR-550a-3-5p/YAP signaling, the YAP-5SA active mutant (33) (serine-to-alanine mutation at all putative LATS kinase phosphorylation sites on YAP including S61A, S109A, S127/128A, S131A, S163/164A, and S381A, thus leading to constitutive YAP activation) was used in the miR-550a-3-5p-overexpressed HPV-positive cells. YAP-5SA transfection obviously rescued miR-550a-3-5p-induced repression of CCL2, which identified the role of miR-550a-3-5p/YAP in regulating CCL2 expression (Fig. 5F). Furthermore, classical target genes of YAP were also detected (34), and the ability of YAP-5SA rescuing miR-550a-3-5p-induced repression of CCNE2 and CDC6 might indicate the reason why miR-550a-3-5p affected proliferation and apoptosis in OSCC cells (Supplementary Fig. 3C).

CCL2 is a well-established chemokine important for the recruitment of macrophages (35). Accordingly, we examined whether the role of miR-550a-3-5p in inhibiting migration, invasion and EMT of HPV-positive OSCC cells was dependent on YAP/CCL2-induced M2 macrophages infiltration. In CM from HPV-positive OSCC cells, miR-550a-3-5p overexpression or YAP knockdown significantly abrogated expressions of M2 macrophages marker CD163 on PMA-induced THP-1 cells, whereas YAP-activation using YAP-5SA in miR-550a-3-5p-overexpressed cells or adding recombinant human CCL2 protein to miR-550a-3-5p-overexpressed or YAP-knockdown cells could rescue CD163 expressions (Fig. 5G). Then, after co-culturing with these CM-induced TMAs for 48 h, we found that increased mRNA expressions of E-cadherin in both UPCI:SCC090 and UM-SCC-47 cells by miR-550a-3-5p overexpression or YAP knockdown were mostly abolished when co-transfected with YAP-5SA or added CCL2. Completely opposite results were observed in Vimentin expressions, and protein levels of E-cadherin and Vimentin were confirmed by Western blot, suggesting that the effects of miR-550a-3-5p on inhibiting EMT of HPV-positive OSCC cells were dependent on suppression of YAP/CCL2-mediated M2 macrophages polarization (Fig. 5H).

Verteporfin treatment inhibited tumor development in E6-E7 knock-in mice with 4NQO-induced OSCC

VP, previously identified as a transcriptional inhibitor of YAP, was assessed in a 4NQO-induced model of OSCC in Rosa26-E6-E7 constitutive knock-in mice. After 8 weeks of drinking water with 4NQO and 8 weeks with distilled water, VP was injected intraperitoneally at 3-day intervals, and the mice were assessed after 6 doses of VP (Fig. 6A). Results showed that tongue lesions caused by 4NQO treatment

were more obvious in vehicle-treated mice than VP-treated mice. A total of 62.5% (5/8) mice showed lesions in both VP and Vehicle group, while the tumor size was (1.70 ± 0.97) mm on average in VP group and (2.59 ± 0.82) mm in Vehicle group, and the average number of lesions per mouse was 1.00 in VP group and (2.20 ± 1.09) in Vehicle group (Fig. 6B, C). These revealed that VP weakened the formation of tongue lesions induced by 4NQO.

Then, HE staining demonstrated that the tumors present in the VP-treated mice were minimally dysplastic as compared to the more advanced in Vehicle-treated mice (Fig. 6D). Results of histopathological analysis of VP and Vehicle group were described in Table 2, which showed that in VP group, 37.5% of the mice exhibited a high risk of oral carcinogenesis, with respect to 62.5% of the mice in Vehicle group, according to a previously reported two-category system (normal/hyperplasia/mild or moderate dysplasia: low risk; severe dysplasia/carcinoma: high risk) (36). In addition, a significant decrease in the expression of CCL2 and CD163 was observed in tumors from VP-treated mice (Fig. 6E). These indicated that VP suppressed the 4NQO-induced tongue carcinogenesis by down-regulating CCL2 production and M2 macrophages in transgenic mice with E6/7 knock-in.

Table 2
Histopathological examination of tongue lesions in various 4NQO-treated mice groups

Group	Mice No.	Normal epithelial	Hyperplasia	Dysplasia			Squamous cell carcinoma
				Mild	Moderate	Severe	
Vehicle	8	0	1(12.5%)	1(12.5%)	1(12.5%)	1(12.5%)	4(50%)
VP	8	0	2(25%)	1(12.5%)	2(25%)	2(25%)	1(12.5%)

Correlations of miR-550a-3-5p, YAP, CCL2 and M2 macrophages in vivo and in HPV-positive OSCC patients

We investigated the expression of YAP, CCL2 and CD163 in miR-550a-3-5p-overexpressed HPV-positive OSCC cells-derived xenografts of nude mice. Results of immunohistochemistry staining showed that miR-550a-3-5p overexpression was significantly correlated with decreased nuclear-stained of active YAP, cytoplasmic-stained of CCL2 and CD163. Consistently, miR-550a-3-5p overexpression was associated with decreased mRNA levels of YAP, CCL2 and CD163 (Fig. 7A, B). Furthermore, staining of active YAP, CCL2 and CD163 were also carried out in 25 cases of HPV-positive OSCC specimens which we have used in analyzing miR-550a-3-5p expression. As shown in Fig. 7C, patient 1 referred to representative case with low miR-550a-3-5p expression, while patient 2 had higher miR-550a-3-5p expression. Similarly, low miR-550a-3-5p expressions tended to be associated with high levels of YAP and CCL2, and more M2 macrophages infiltration in HPV-positive OSCC patients (Fig. 7D).

Discussion

Previous researches have evidently certificated that even though HPV-positive OSCC presents a relatively better prognosis in most cases, it usually exhibits an aggressive behavior with lymph nodes already being metastasized. (37). Wakisaka et al. have showed that in clinical specimens of OPSCC, HPV positivity was significantly correlated with EMT induction, which was defined by E-cadherin-negative and Vimentin-positive. Furthermore, these EMT-positive cases showed more relevance with advanced nodal status. (38). Mechanistically, a study has revealed that HPV 16 E7 oncoprotein expression in keratinocytes could epigenetically repress the E-cadherin expression by augmenting cellular DNA methyltransferase I activity (39). In addition, a research team used trophoblastic cells to investigate oncogenic roles of HPV16, and results have showed that E5, together with E6 and E7 could impair cell adhesion, and promote migrative and invasive properties via inhibiting E-cadherin expression (40). Moreover, there was a study having reported that HPV16 E6 and E7 could induce EMT-relevant molecular alterations independently through non-transcriptional ways, thus leading to malignant progression of epithelial cells (41). Consistently, our study found that in HPV-positive OSCC cells, the effects of miR-550a-3-5p on suppressing M2 macrophages polarization, and thus migration, invasion and EMT phenotype relied on the regulation of its upstream factor E6 oncoprotein. This described at least in part the mechanisms by which E6 promoted EMT of HPV-positive OSCC.

The tumor microenvironment has emerged to be a critical part in the process of cancer metastasis. Even though lots of previous studies have only concentrated on the intrinsic mechanisms of miRNAs in cancer cells, the miRNAs-mediated crosstalks between cancer cells and tumor microenvironment which could also affect cancer metastasis have recently been investigated (42). For example, miR-141-3p was reported to inhibit normal fibroblasts' transition to cancer-associated fibroblasts via STAT4/wnt/β-catenin pathway, thus leading to suppressed migration and invasion in gastric cancer cells (43). Additionally, highly expressed miR-301a-3p, induced by hypoxia in pancreatic cancer cells, could mediate M2 macrophages polarization to promote cancer metastasis via direct exosome delivery (44). Also in this study, we found a signaling pathway that influenced tumor microenvironment and was mediated by miR-550a-3-5p, which modulated TAMs polarization and in turn affected migration, invasion, and EMT of HPV-positive OSCC cells.

miR-550 has been reported to be differentially expressed in several types of cancers and exert important regulatory effects on cancer development. In non-small cell lung cancer, Yang and colleagues have showed that miR-550a-3p was highly expressed and promoted proliferation, migration and invasion of cancer cells by targeting TIMP2 (45). In colorectal cancer cells, miR-550a-5p was inversely regulated by tumor suppressor Brg-1, and promoted migration and invasion via RNF43/Wnt/β-catenin pathway (46). Moreover, miR-550a could also enhance metastasis in hepatocellular carcinoma through down-regulating CPEB4 expression (47). However, due to the tissue specificity, miR-550 also exerts tumor-suppressor roles. For example, down-regulated miR-550a-3p led to the initiation, growth and metastasis of breast cancer by promoting ERK1/2 levels (48). The same as our findings, miR-550a-3-5p was negatively associated with the growth and metastatic potential of both HPV-positive and negative OSCC cells. Down-regulation of miR-550a-3-5p indicated higher tumor size and nodal metastasis of HPV-positive OSCC patients, suggesting its anti-tumor role especially in HPV-positive OSCC. Furthermore, unlike in other types of

cancer, though its inhibitory roles in HPV-negative OSCC and in growth of HPV-positive OSCC might derive from direct mechanisms which need further investigation, miR-550a-3-5p affected migration and invasion of HPV-positive OSCC cells indirectly as the discrepancy between in vivo and in vitro studies. Thus, here we aimed to search for the downstream pathways of miR-550a-3-5p and verify whether these molecules resulted in the indirect tumor-suppressive influences of miR-550a-3-5p. Through bioinformatics analysis, gene expression patterns and dual luciferase reporter gene assays, we found that miR-550a-3-5p directly targeted YAP which emerged to exhibit great roles in cancer immunity, and further regulated M2 macrophages polarization and migration, invasion and EMT of HPV-positive OSCC cells via YAP/CCL2 signaling. Similarly, a recent study also reported that miR-550a-3-5p could directly target YAP to exert tumor-suppressor roles in various cancers containing colon cancer, breast cancer, lung cancer, and head and neck cancer (49). However, this didn't include OSCC cell lines and only concentrated on the direct effects of miR-550a-3-5p.

YAP, as a central effector of the Hippo pathway and a transcriptional co-activator with TAZ, takes great part in controlling organ size, development, and tumorigenesis (50, 51). Canonically, core kinase cascade of the Hippo pathway Mst1/2-Lats1/2 is responsible for phosphorylation of YAP/TAZ, which then leads to its cytoplasmic retention, ubiquitination and degradation (52). However, there are also non-canonical pathways that promote nucleus-translocation of YAP/TAZ, and thus stimulate its transcriptional activities, through which YAP/TAZ plays important tumor-promoting roles in a number of cancers (53). Several studies have also showed that aberrant YAP accumulation in the nucleus of cancer cells was found in both cervical cancer and HPV-positive OSCC, and HPV-positive patients with higher YAP levels usually had a more advanced stage (54–56). Moreover, Webb Strickland and colleagues have reported that E6 oncoprotein could associate with cellular PDZ domain proteins to promote the nuclear localization of YAP (57). In our study, we put forward a pathway in which miR-550a-3-5p, down-regulated by E6 oncoprotein, inhibited YAP but not TAZ in HPV-positive OSCC. Then, we found that YAP inhibition could suppress cancer progression using YAP inhibitor Verteporfin in 4NQO-induced OSCC model of E6-E7 knock-in mice. These results were consistent with the relatively high expression of YAP and its tumor-promoting role in HPV-positive cancers.

The transcriptional activities of YAP/TAZ are mainly conducted by binding to the TEAD family and thus promoting the expression of genes critical for cancer cell proliferation, survival and stemness (58). We have detected its classical target genes including CTGF, CYR61, CCNE2, CDC6 and CDK2 in our study, and only CCNE2 and CDC6 were up-regulated in YAP-activated HPV-positive OSCC cells, while miR-550a-3-5p overexpression could weaken these effects. These may partly explain the mechanism by which miR-550a-3-5p regulated proliferation and apoptosis of cancer cells. However, no significant changes were observed in expressions of other canonical target genes, which may ascribe to the different context in HPV-positive OSCC, according to a recent article studying the molecular signature regulated by YAP/TAZ in OSCC cells (34). Recently, accumulating evidence suggests that the effect of YAP is not confined to cancer cells, but instead involves the regulation of cancer immune microenvironment. Secretion of certain cytokines or chemokines by cancer cells could be modulated owing to increased YAP activity, thus recruiting myeloid-derived suppressive cell (MDSCs) or M2 macrophages and inhibiting anti-tumor

immunity (28–30). In line with this, we found that YAP, down-regulated by miR-550a-3-5p, could promote CCL2 expression transcriptionally by interaction with TEAD family, thus contributing to M2 macrophages polarization.

CCL2 is a highly expressed chemokine in cancer cells and secreted to contribute to cancer progression (59, 60). In addition, CCL2 also enhances TAMs infiltration and exerts tumor-promoting effects indirectly (61). For example, in hepatocellular carcinoma, FoxQ1 could promote TAMs infiltration via the VersicanV1/CCL2 axis (62). Moreover, in breast cancer, CCL2, produced by cancer cells, could continually recruit inflammatory monocytes and promote their differentiation into TAMs, which facilitated the subsequent growth of metastatic cells (63). Our results revealed that E6/miR-550a-3-5p/YAP could promote M2 macrophages polarization through increasing CCL2, and thus led to the enhanced EMT in HPV-positive OSCC cells. As shown in Fig. 7E, Findings of our studies were summarized in a schematic.

Conclusion

Taken together, E6/miR-550a-3-5p/YAP/CCL2 is a novel signaling axis identified in HPV-positive OSCC and involved in mediation of crosstalk between cancer cells and macrophages. Although this signaling pathway concerns complicated immune networks that need to be studied further in detail, miR-550a-3-5p overexpression combined with YAP inhibition or immunotherapy might be a new strategy for advanced HPV-positive OSCC.

Abbreviations

CM, conditioned media; DOK, dysplasia human oral keratinocytes; EMT, epithelial-mesenchymal transition; FISH, fluorescence in situ hybridization; HPV, Human papillomavirus; IHC, Immunohistochemistry; miRNA, microRNA; MUT, mutant; NOK, normal human oral keratinocytes; OSCC, oral squamous cell carcinoma; siRNA, small-interfering RNA; TAM, tumor-associated macrophage; VP, verteporfin; WT, wild type.

Declarations

Competing interests

The authors declare that there are no competing interests.

Acknowledgement

We thank Dr. Fanyuan Yu from West China School of Stomatology, Sichuan University for providing the plasmid pCDH-EF1-YAP-5SA (FLAG-tagged) and the empty Vector.

Author contributions

MXC, WLZ, XHL and YLT designed the research study. MXC, XWQ, MCH, KW and JBW conducted the experiments on the human samples. MXC, WLZ, XHY, JSW and JJ conducted the cell experiments and animal studies. MXC, YJT and JJ were involved in data analysis. MXC were responsible for writing of manuscript. All authors reviewed the manuscript.

Funding

Financial supports are from the National Key R&D Program of China (No. 2019YFA09005700), and National Natural Science Foundation of China grants (Nos. 81672672, 81972542,1902779 and 21838002).

Availability of data and materials

The data that support the findings of this study are available from the corresponding author upon reasonable request.

Ethics approval and consent to participate

This research was conducted under the approval and supervision of the Institutional Ethics Committee of the West China Medical Center, Sichuan University, China. Animal study was undertaken with the approval of the Institutional Animal Care and Use Committee of West China Medical Center, Sichuan University, China.

Consent for publication

All authors agreed on the publication of this manuscript.

References

1. Bray F, Ferlay J, Soerjomataram I, Siegel RL, Torre LA, Jemal A. Global cancer statistics 2018: GLOBOCAN estimates of incidence and mortality worldwide for 36 cancers in 185 countries. CA: a cancer journal for clinicians. 2018 Nov;68(6):394-424.
2. Maxwell JH, Grandis JR, Ferris RL. HPV-Associated Head and Neck Cancer: Unique Features of Epidemiology and Clinical Management. Annu Rev Med. 2016;67.
3. Westra WH. The pathology of HPV-related head and neck cancer: implications for the diagnostic pathologist. Semin Diagn Pathol. 2015;32(1):42-53.
4. Fakhry C, Westra WH, Wang SJ, van Zante A, Zhang Y, Rettig E, et al. The prognostic role of sex, race, and human papillomavirus in oropharyngeal and nonoropharyngeal head and neck squamous cell cancer. Cancer. 2017;123(9):1566-75.
5. Ang KK, Harris J, Wheeler R, Weber R, Rosenthal DI, Nguyen-Tan PF, et al. Human papillomavirus and survival of patients with oropharyngeal cancer. The New England journal of medicine. 2010 Jul 1;363(1):24-35.

6. Posner MR, Lorch JH, Goloubeva O, Tan M, Schumaker LM, Sarlis NJ, et al. Survival and human papillomavirus in oropharynx cancer in TAX 324: a subset analysis from an international phase III trial. Ann Oncol. 2011;22(5):1071-7.
7. Vainshtein JM, Spector ME, McHugh JB, Wong KK, Walline HM, Byrd SA, et al. Refining risk stratification for locoregional failure after chemoradiotherapy in human papillomavirus-associated oropharyngeal cancer. Oral Oncol. 2014;50(5):513-9.
8. Chaffer CL, Weinberg RA. A perspective on cancer cell metastasis. Science. 2011;331(6024):1559-64.
9. Grigore AD, Jolly MK, Jia D, Farach-Carson MC, Levine H. Tumor Budding: The Name is EMT. Partial EMT. J Clin Med. 2016;5(5).
10. Qian B-Z, Pollard JW. Macrophage diversity enhances tumor progression and metastasis. Cell. 2010;141(1):39-51.
11. Goswami KK, Ghosh T, Ghosh S, Sarkar M, Bose A, Baral R. Tumor promoting role of anti-tumor macrophages in tumor microenvironment. Cell Immunol. 2017;316.
12. Weng YS, Tseng HY, Chen YA, Shen PC, Al Haq AT, Chen LM, et al. MCT-1/miR-34a/IL-6/IL-6R signaling axis promotes EMT progression, cancer stemness and M2 macrophage polarization in triple-negative breast cancer. Molecular cancer. 2019 Mar 18;18(1):42.
13. Li L, Sun P, Zhang C, Li Z, Cui K, Zhou W. MiR-98 modulates macrophage polarization and suppresses the effects of tumor-associated macrophages on promoting invasion and epithelial-mesenchymal transition of hepatocellular carcinoma. Cancer cell international. 2018;18:95.
14. Sasahira T, Kurihara M, Yamamoto K, Ueda N, Nakashima C, Matsushima S, et al. HuD promotes progression of oral squamous cell carcinoma. Pathobiology : journal of immunopathology, molecular and cellular biology. 2014;81(4):206-14.
15. Chen X, Yan B, Lou H, Shen Z, Tong F, Zhai A, et al. Immunological network analysis in HPV associated head and neck squamous cancer and implications for disease prognosis. Mol Immunol. 2018;96:28-36.
16. Bartel DP. MicroRNAs: genomics, biogenesis, mechanism, and function. Cell. 2004 Jan 23;116(2):281-97.
17. Zhang Y, Yang P, Wang X-F. Microenvironmental regulation of cancer metastasis by miRNAs. Trends Cell Biol. 2014;24(3):153-60.
18. Croce CM. Causes and consequences of microRNA dysregulation in cancer. Nat Rev Genet. 2009;10(10):704-14.
19. Božinović K, Sabol I, Dediol E, Milutin Gašperov N, Manojlović S, Vojtechova Z, et al. Genome-wide miRNA profiling reinforces the importance of miR-9 in human papillomavirus associated oral and oropharyngeal head and neck cancer. Scientific reports. 2019;9(1):2306.
20. Hui AB, Lin A, Xu W, Waldron L, Perez-Ordonez B, Weinreb I, et al. Potentially prognostic miRNAs in HPV-associated oropharyngeal carcinoma. Clinical cancer research : an official journal of the American Association for Cancer Research. 2013 Apr 15;19(8):2154-62.

21. Zheng M, Cao M-X, Luo X-J, Li L, Wang K, Wang S-S, et al. EZH2 promotes invasion and tumour glycolysis by regulating STAT3 and FoxO1 signalling in human OSCC cells. J Cell Mol Med. 2019;23(10):6942-54.
22. Chen X, Fu E, Lou H, Mao X, Yan B, Tong F, et al. IL-6 induced M1 type macrophage polarization increases radiosensitivity in HPV positive head and neck cancer. Cancer letters. 2019;456:69-79.
23. Wu J-S, Li L, Wang S-S, Pang X, Wu J-B, Sheng S-R, et al. Autophagy is positively associated with the accumulation of myeloid-derived suppressor cells in 4-nitroquinoline-1-oxide-induced oral cancer. Oncol Rep. 2018;40(6):3381-91.
24. Brabletz T, Kalluri R, Nieto MA, Weinberg RA. EMT in cancer. Nature reviews Cancer. 2018 Feb;18(2):128-34.
25. Zhou SL, Hu ZQ, Zhou ZJ, Dai Z, Wang Z, Cao Y, et al. miR-28-5p-IL-34-macrophage feedback loop modulates hepatocellular carcinoma metastasis. Hepatology (Baltimore, Md). 2016 May;63(5):1560-75.
26. Sano D, Oridate N. The molecular mechanism of human papillomavirus-induced carcinogenesis in head and neck squamous cell carcinoma. International journal of clinical oncology. 2016 Oct;21(5):819-26.
27. Zhang Y, Zhang H, Zhao B. Hippo Signaling in the Immune System. Trends in biochemical sciences. 2018 Feb;43(2):77-80.
28. Kim W, Khan SK, Liu Y, Xu R, Park O, He Y, et al. Hepatic Hippo signaling inhibits protumoural microenvironment to suppress hepatocellular carcinoma. Gut. 2018 Sep;67(9):1692-703.
29. Guo X, Zhao Y, Yan H, Yang Y, Shen S, Dai X, et al. Single tumor-initiating cells evade immune clearance by recruiting type II macrophages. Genes & development. 2017 Feb 1;31(3):247-59.
30. Wang G, Lu X, Dey P, Deng P, Wu CC, Jiang S, et al. Targeting YAP-Dependent MDSC Infiltration Impairs Tumor Progression. Cancer discovery. 2016 Jan;6(1):80-95.
31. Moroishi T, Hayashi T, Pan WW, Fujita Y, Holt MV, Qin J, et al. The Hippo Pathway Kinases LATS1/2 Suppress Cancer Immunity. Cell. 2016 Dec 1;167(6):1525-39 e17.
32. Liu-Chittenden Y, Huang B, Shim JS, Chen Q, Lee SJ, Anders RA, et al. Genetic and pharmacological disruption of the TEAD-YAP complex suppresses the oncogenic activity of YAP. Genes & development. 2012 Jun 15;26(12):1300-5.
33. Wang W, Xiao Z-D, Li X, Aziz KE, Gan B, Johnson RL, et al. AMPK modulates Hippo pathway activity to regulate energy homeostasis. Nat Cell Biol. 2015;17(4):490-9.
34. Hiemer SE, Zhang L, Kartha VK, Packer TS, Almershed M, Noonan V, et al. A YAP/TAZ-Regulated Molecular Signature Is Associated with Oral Squamous Cell Carcinoma. Molecular cancer research : MCR. 2015 Jun;13(6):957-68.
35. Chen C, He W, Huang J, Wang B, Li H, Cai Q, et al. LNMAT1 promotes lymphatic metastasis of bladder cancer via CCL2 dependent macrophage recruitment. Nature communications. 2018 Sep 20;9(1):3826.

36. Warnakulasuriya S, Reibel J, Bouquot J, Dabelsteen E. Oral epithelial dysplasia classification systems: predictive value, utility, weaknesses and scope for improvement. Journal of oral pathology & medicine : official publication of the International Association of Oral Pathologists and the American Academy of Oral Pathology. 2008;37(3):127-33.
37. Fakhry C, Westra WH, Li S, Cmelak A, Ridge JA, Pinto H, et al. Improved survival of patients with human papillomavirus-positive head and neck squamous cell carcinoma in a prospective clinical trial. Journal of the National Cancer Institute. 2008;100(4):261-9.
38. Wakisaka N, Yoshida S, Kondo S, Kita M, Sawada-Kitamura S, Endo K, et al. Induction of epithelial-mesenchymal transition and loss of podoplanin expression are associated with progression of lymph node metastases in human papillomavirus-related oropharyngeal carcinoma. Histopathology. 2015;66(6):771-80.
39. Laurson J, Khan S, Chung R, Cross K, Raj K. Epigenetic repression of E-cadherin by human papillomavirus 16 E7 protein. Carcinogenesis. 2010;31(5):918-26.
40. Boulenouar S, Weyn C, Van Noppen M, Moussa Ali M, Favre M, Delvenne PO, et al. Effects of HPV-16 E5, E6 and E7 proteins on survival, adhesion, migration and invasion of trophoblastic cells. Carcinogenesis. 2010;31(3):473-80.
41. Hellner K, Mar J, Fang F, Quackenbush J, Münger K. HPV16 E7 oncogene expression in normal human epithelial cells causes molecular changes indicative of an epithelial to mesenchymal transition. Virology. 2009;391(1):57-63.
42. Rupaimoole R, Calin GA, Lopez-Berestein G, Sood AK. miRNA Deregulation in Cancer Cells and the Tumor Microenvironment. Cancer discovery. 2016;6(3):235-46.
43. Zhou Y, Zhong J-H, Gong F-S, Xiao J. MiR-141-3p suppresses gastric cancer induced transition of normal fibroblast and BMSC to cancer-associated fibroblasts via targeting STAT4. Exp Mol Pathol. 2019;107:85-94.
44. Wang X, Luo G, Zhang K, Cao J, Huang C, Jiang T, et al. Hypoxic Tumor-Derived Exosomal miR-301a Mediates M2 Macrophage Polarization via PTEN/PI3Kγ to Promote Pancreatic Cancer Metastasis. Cancer research. 2018;78(16):4586-98.
45. Yang JZ, Bian L, Hou JG, Wang HY. MiR-550a-3p promotes non-small cell lung cancer cell proliferation and metastasis through down-regulating TIMP2. European review for medical and pharmacological sciences. 2018;22(13):4156-65.
46. Wang G, Fu Y, Yang X, Luo X, Wang J, Gong J, et al. Brg-1 targeting of novel miR550a-5p/RNF43/Wnt signaling axis regulates colorectal cancer metastasis. Oncogene. 2016 Feb 04;35(5):651-61.
47. Tian Q, Liang L, Ding J, Zha R, Shi H, Wang Q, et al. MicroRNA-550a acts as a pro-metastatic gene and directly targets cytoplasmic polyadenylation element-binding protein 4 in hepatocellular carcinoma. PloS one. 2012;7(11):e48958.
48. Ho JY, Hsu RJ, Wu CH, Liao GS, Gao HW, Wang TH, et al. Reduced miR-550a-3p leads to breast cancer initiation, growth, and metastasis by increasing levels of ERK1 and 2. Oncotarget. 2016 Aug 16;7(33):53853-68.

49. Choe MH, Yoon Y, Kim J, Hwang SG, Han YH, Kim JS. miR-550a-3-5p acts as a tumor suppressor and reverses BRAF inhibitor resistance through the direct targeting of YAP. Cell death & disease. 2018 May 29;9(6):640.
50. Dong J, Feldmann G, Huang J, Wu S, Zhang N, Comerford SA, et al. Elucidation of a universal size-control mechanism in Drosophila and mammals. Cell. 2007;130(6):1120-33.
51. Yu F-X, Zhao B, Guan K-L. Hippo Pathway in Organ Size Control, Tissue Homeostasis, and Cancer. Cell. 2015;163(4):811-28.
52. White SM, Murakami S, Yi C. The complex entanglement of Hippo-Yap/Taz signaling in tumor immunity. Oncogene. 2019 Jan 7.
53. Pan D. The hippo signaling pathway in development and cancer. Dev Cell. 2010;19(4):491-505.
54. Alzahrani F, Clattenburg L, Muruganandan S, Bullock M, MacIsaac K, Wigerius M, et al. The Hippo component YAP localizes in the nucleus of human papilloma virus positive oropharyngeal squamous cell carcinoma. Journal of otolaryngology - head & neck surgery = Le Journal d'oto-rhino-laryngologie et de chirurgie cervico-faciale. 2017 Feb 22;46(1):15.
55. He C, Mao D, Hua G, Lv X, Chen X, Angeletti PC, et al. The Hippo/YAP pathway interacts with EGFR signaling and HPV oncoproteins to regulate cervical cancer progression. EMBO molecular medicine. 2015 Nov;7(11):1426-49.
56. Xiao H, Wu L, Zheng H, Li N, Wan H, Liang G, et al. Expression of Yes-associated protein in cervical squamous epithelium lesions. International journal of gynecological cancer : official journal of the International Gynecological Cancer Society. 2014 Nov;24(9):1575-82.
57. Webb Strickland S, Brimer N, Lyons C, Vande Pol SB. Human Papillomavirus E6 interaction with cellular PDZ domain proteins modulates YAP nuclear localization. Virology. 2018 Mar;516:127-38.
58. Moon S, Yeon Park S, Woo Park H. Regulation of the Hippo pathway in cancer biology. Cell Mol Life Sci. 2018;75(13):2303-19.
59. Bonapace L, Coissieux M-M, Wyckoff J, Mertz KD, Varga Z, Junt T, et al. Cessation of CCL2 inhibition accelerates breast cancer metastasis by promoting angiogenesis. Nature. 2014;515(7525):130-3.
60. Park SI, Liao J, Berry JE, Li X, Koh AJ, Michalski ME, et al. Cyclophosphamide creates a receptive microenvironment for prostate cancer skeletal metastasis. Cancer research. 2012;72(10):2522-32.
61. Li X, Yao W, Yuan Y, Chen P, Li B, Li J, et al. Targeting of tumour-infiltrating macrophages via CCL2/CCR2 signalling as a therapeutic strategy against hepatocellular carcinoma. Gut. 2017;66(1):157-67.
62. Xia L, Huang W, Tian D, Zhang L, Qi X, Chen Z, et al. Forkhead box Q1 promotes hepatocellular carcinoma metastasis by transactivating ZEB2 and VersicanV1 expression. Hepatology (Baltimore, Md). 2014;59(3):958-73.
63. Linde N, Casanova-Acebes M, Sosa MS, Mortha A, Rahman A, Farias E, et al. Macrophages orchestrate breast cancer early dissemination and metastasis. Nature communications. 2018;9(1):21.

Additional Files

Additional file 1: Supplementary Fig. 1. (A) Representative images showed PCR-based detection of HPV-16/18 DNA from OSCC samples. **(B)** miR-550a-3-5p was down-regulated in p16-positive OPSCC samples according to a previous study (reference 20). **(C)** miR-550a-3-5p expressions were evaluated using qRT-PCR in different oral cell lines (NOK, normal oral keratinocytes; DOK, dysplasia oral keratinocytes; Cal-27, SCC25 and HSC3, HPV-negative OSCC cell lines; UPCI:SCC090 and UM-SCC-47, HPV-positive OSCC cell lines). **(D)** miR-550a-3-5p expressions were detected by qRT-PCR after transfected with miR-550a-3-5p mimic, mimic NC, inhibitor, inhibitor NC in Cal-27, SCC25, UPCI:SCC090 and UM-SCC-47 cell lines. **(E)** miR-550a-3-5p expressions were detected by qRT-PCR after stably transfected with miR-550a-3-5p lentiviral vector (GFP-tagged) in Cal-27 and UPCI:SCC090 cell lines. Representative images showed transfected cells with GFP fluorescence (magnification 200X). **(F)** Representative images of H&E staining and miR-550a-3-5p FISH in xenografts derived from miR-550a-3-5p-overexpressed Cal-27 and UPCI:SCC090 cell lines. Nucleus was stained blue by DAPI, and miR-550a-3-5p was stained red (magnification 400X). All assays were carried out in triplicate. Results were presented as means ± SD. **P* 0.05, ***P* 0.01, ****P* 0.001.

Additional file 2: Supplementary Fig. 2. miR-550a-3-5p inhibited proliferation and enhanced apoptosis in HPV-positive and HPV-negative OSCC cells. (A) CCK-8 assays of HPV-positive OSCC cells (UPCI:SCC090 and UM-SCC-47) and HPV-negative OSCC cells (Cal-27 and SCC25) with miR-550a-3-5p overexpression (M, mimic-transfected) or inhibition (I, inhibitor-transfected). **(B)** Flow cytometry-based apoptosis analysis was used to examine the percentage of apoptotic cells in HPV-positive and HPV-negative OSCC cells with miR-550a-3-5p overexpression or inhibition. All assays were carried out in triplicate.

Additional file 3: Supplementary Fig. 3. (A) mRNA levels of E6 and E7 using qRT-PCR in E6 or E7 siRNA-transfected HPV-positive OSCC cells (UPCI:SCC090 and UM-SCC-47). **(B)** mRNA levels of YAP using qRT-PCR in YAP siRNA-transfected HPV-positive OSCC cells. **(C)** mRNA levels of CTGF, CYR61, CCNE2, CDC6, and CDK2 using qRT-PCR in UPCI:SCC090 cells co-transfected with miR-550a-3-5p and YAP-5SA. Protein expressions of Flag-YAP in YAP-5SA-transfected HPV-positive OSCC cells were determined by Western blot (Left panel). **(D)** GO (molecular function) and KEGG (signaling pathway) analysis of miR-550a-3-5p. All assays were carried out in triplicate. Results were presented as means ± SD. **P* 0.05, ***P* 0.01, ****P* 0.001.

Additional file 4: Supplementary Table 1. miRNA microarray results (Fold change ≥2, P□0.05).

Additional file 5: Supplementary data of Specific primers used for qRT-PCR.

Figures

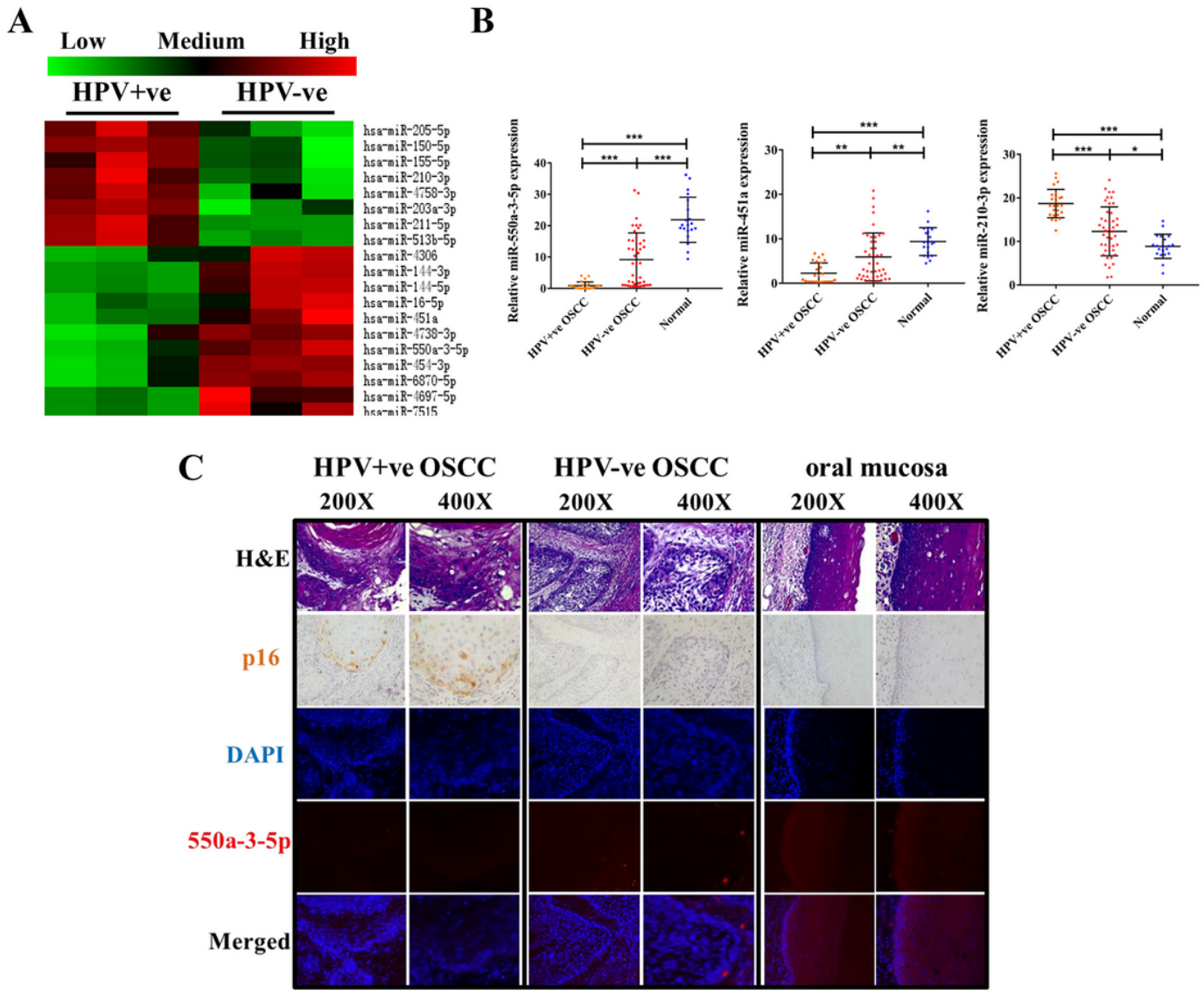

Figure 1

Relative expression of miR-550a-3-5p in HPV-positive OSCC tissue samples. (A) Result of an Agilent human miRNA microarray showed differentially-expressed miRNAs between HPV-positive (n=3) and HPV-negative (n=3) OSCC tissue samples (Fold change ≥2, P 0.05). (B) Relative expressions of miR-550a-3-5p, miR-451a, miR-210-3p in HPV-positive (n=25), HPV-negative (n=45) OSCC tissue samples and normal oral mucosa (n=20) were evaluated by qRT-PCR. (C) Representative FISH images of miR-550a-3-5p in HPV-positive, HPV-negative OSCC tissue samples and normal oral mucosa using formalin-fixed paraffin-embedded sections. H&E staining and IHC staining of p16 were used to confirm tissue types and HPV infection status (magnification 200X, 400X and 1000X). Quantitative analysis based on triplicate experiments. Results were presented as means ± SD. *P 0.05, **P 0.01, ***P 0.001.

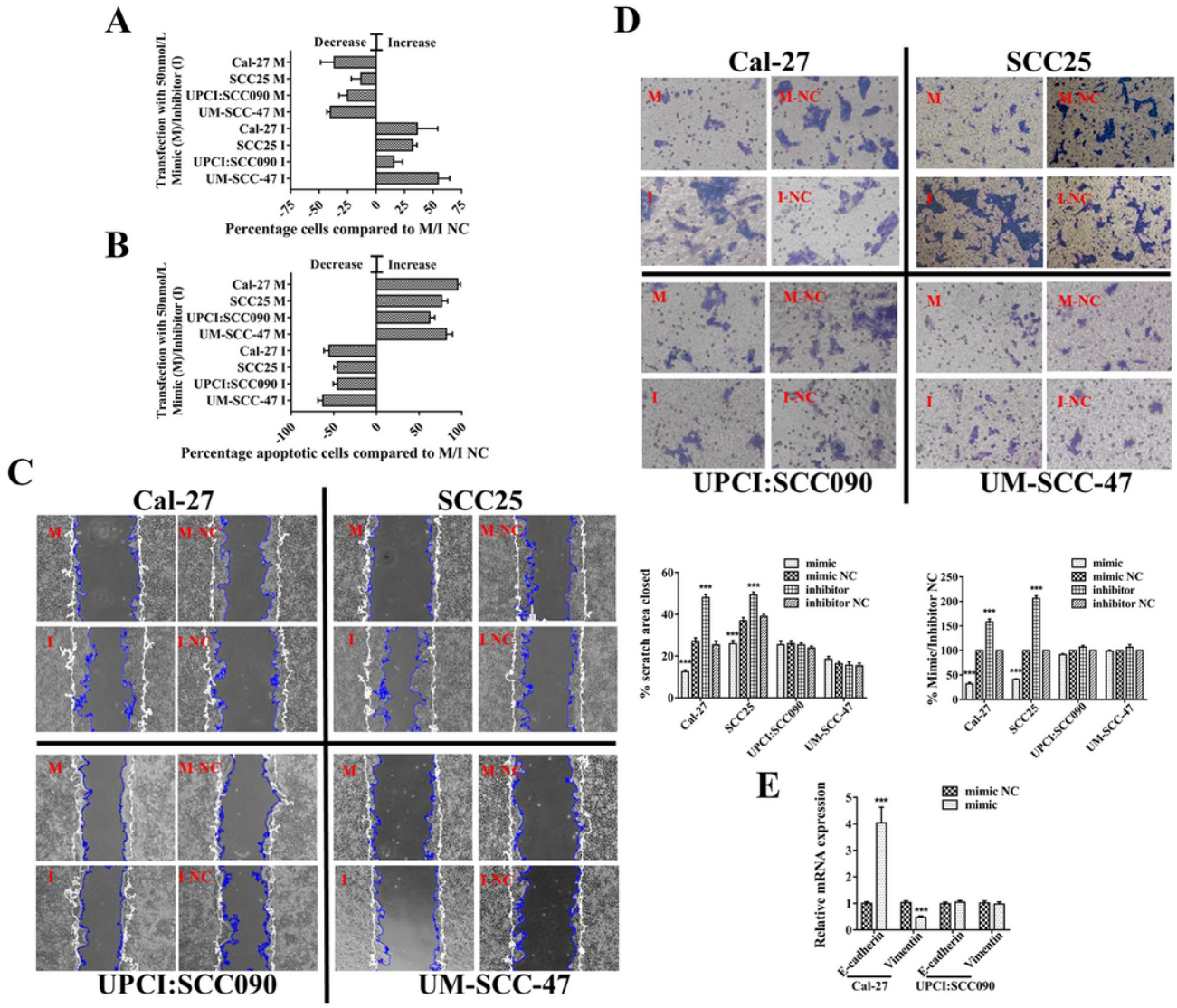

Figure 2

The role of miR-550a-3-5p in regulation of proliferation, apoptosis, migration, invasion, and EMT. (A) Quantitative results of cell proliferation in HPV-positive OSCC cells (UPCI:SCC090 and UM-SCC-47) and HPV-negative OSCC cells (Cal-27 and SCC25) with miR-550a-3-5p overexpression (M, mimic-transfected) or inhibition (I, inhibitor-transfected) were presented by comparing to their NC group. (B) Quantitative results of cell apoptosis in HPV-positive and HPV-negative OSCC cells with miR-550a-3-5p overexpression or inhibition were presented by comparing to their NC group. Images of cell proliferation and flow cytometry were provided in Supplementary Fig. 2 (C) Wound healing assays of HPV-positive and HPV-negative OSCC cells with miR-550a-3-5p overexpression or inhibition. Images were acquired at 0 (white line) and 24 h (blue line) (magnification 200X). Shown were representative images on the left and quantitative analysis of scratch wound closure on the right. (D) Transwell invasion assays of HPV-positive and HPV-negative OSCC cells with miR-550a-3-5p overexpression or inhibition (magnification 200X). Quantification was shown as proportions of their controls. (E) mRNA levels of E-cadherin and Vimentin were assessed in Cal-27 and UPCI:SCC090 cells with miR-550a-3-5p overexpression using qRT-

PCR. All assays were carried out in triplicate. Results were presented as means ± SD. *P 0.05, **P 0.01, ***P 0.001.

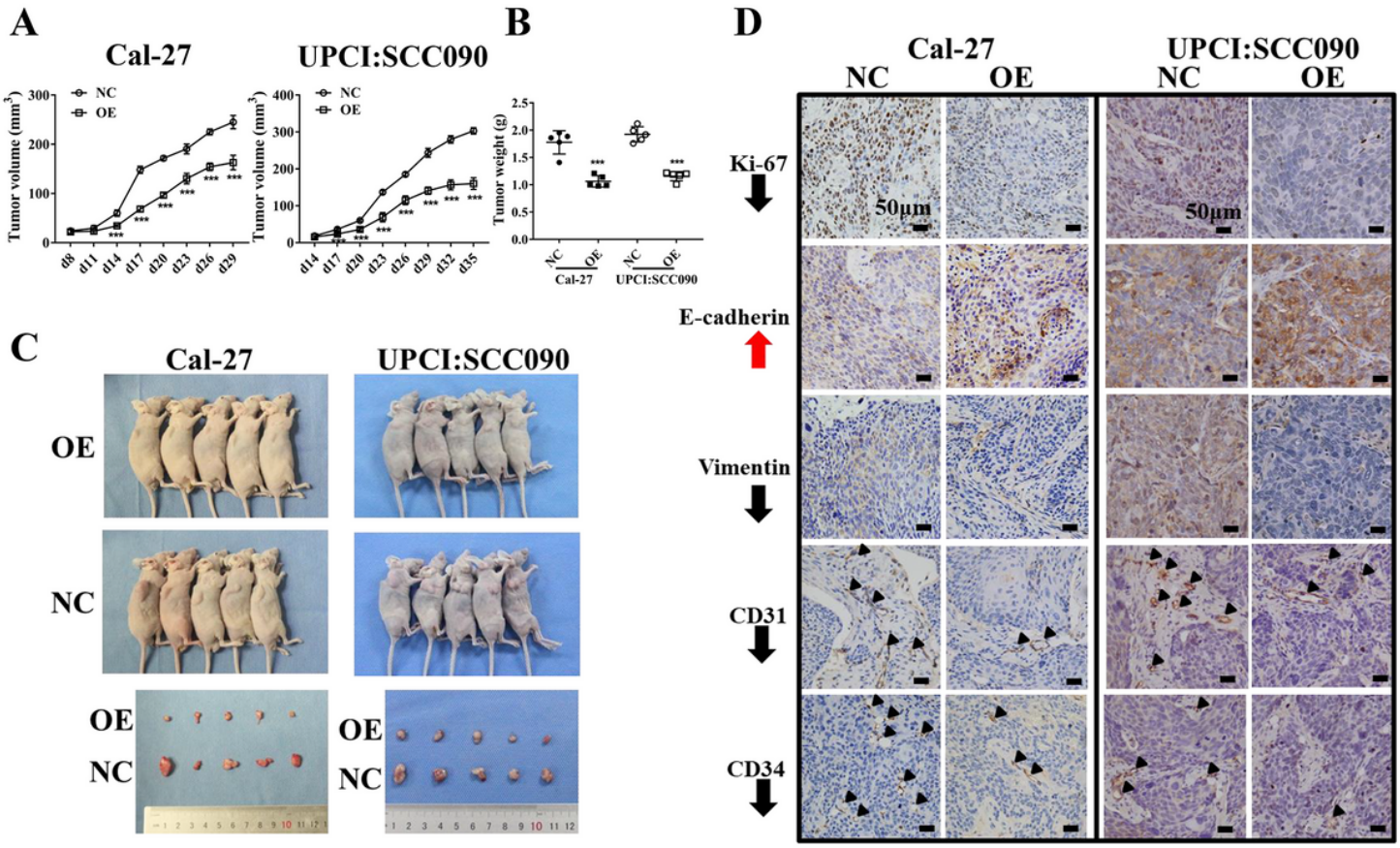

Figure 3

miR-550a-3-5p overexpression suppressed tumor growth and progression in nude mice models. (A to C) Growth curves, weights, and in vivo images of tumors in nude mice xenograft models. (D) Tumor IHC staining revealed the levels of Ki-67, E-cadherin, Vimentin, CD31 and CD34 (indicated by arrowheads). Scale bars, 50 μm. Results were presented as means ± SD. *P 0.05, **P 0.01, ***P 0.001.

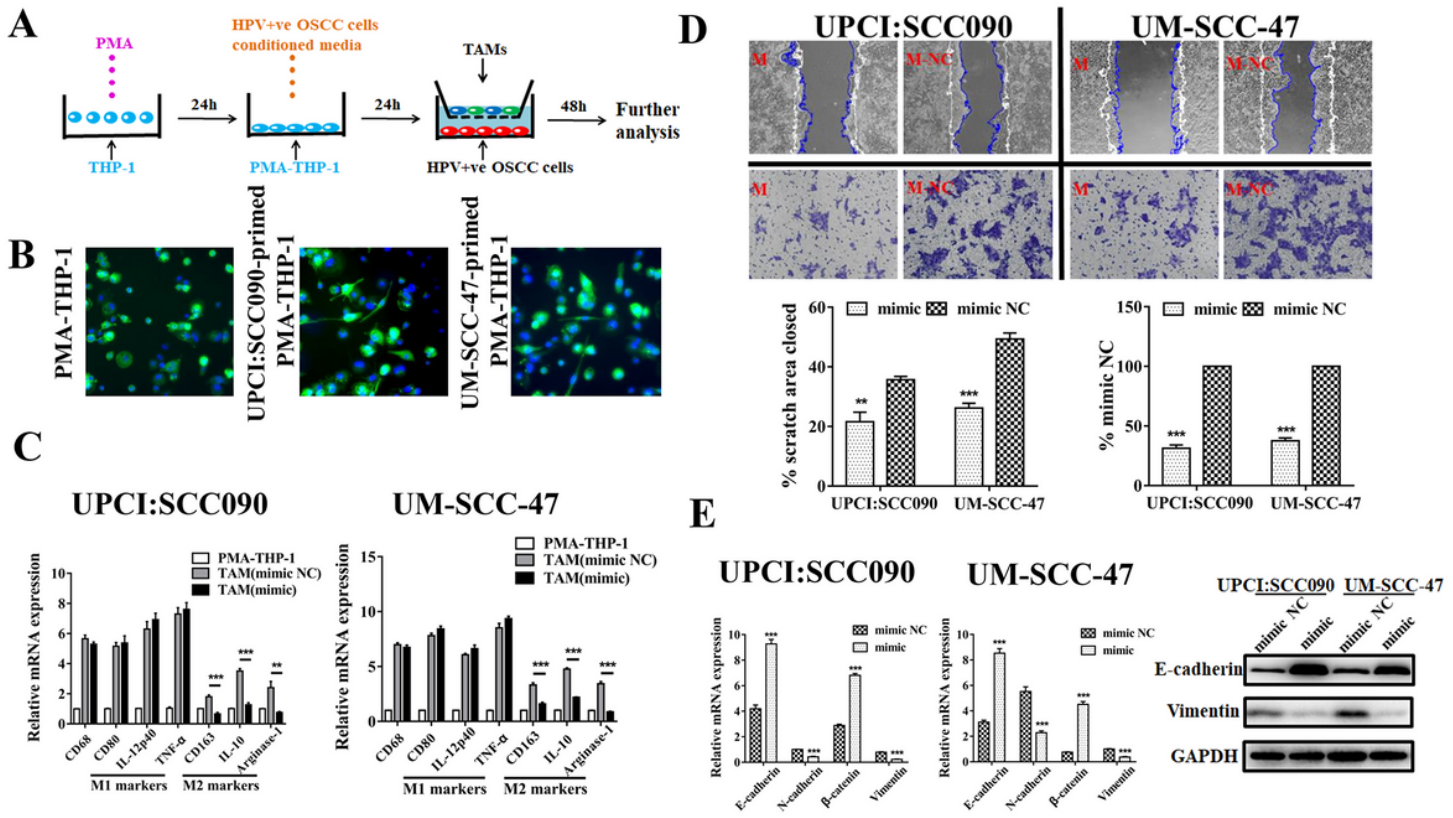

Figure 4

miR-550a-3-5p inhibited M2 macrophages polarization to suppress migration, invasion, and EMT of HPV-positive OSCC cells. (A) Schema for representing the experiment procedures. (B) PMA-induced THP-1 cells were cultured with HPV-positive OSCC cells (UPCI:SCC090 and UM-SCC-47)-conditioned media for 24 h, and morphology was observed using FITC-phalloidin staining (green). Nuclei were stained using DAPI (blue) and PMA-THP-1 cells were used as controls (magnification 200X). (C) qRT-PCR analyzed the expression of the markers of pan-macrophage (CD68), M1 (CD80, IL-12p40, TNF-α) and M2 (CD163, IL-10, Arginase-1) macrophages in PMA-THP-1 cells incubated with CM from miR-550a-3-5p-overexpressed HPV-positive OSCC cells for 24 h. (D) Migration and invasion capacity of miR-550a-3-5p-overexpressed HPV-positive OSCC cells co-cultured with their corresponding TAMs for 48 h were determined by Wound healing and Transwell invasion assay, respectively. Shown were representative images on the upper side with quantitative analysis below (magnification 200X). (E) qRT-PCR for analyzing mRNA levels of E-cadherin, N-cadherin, β-catenin and Vimentin, Western blot for analyzing protein levels of E-cadherin and Vimentin in miR-550a-3-5p-overexpressed HPV-positive OSCC cells co-cultured with their corresponding TAMs for 48 h. All assays were carried out in triplicate. Results were presented as means ± SD. *P 0.05, **P 0.01, ***P 0.001.

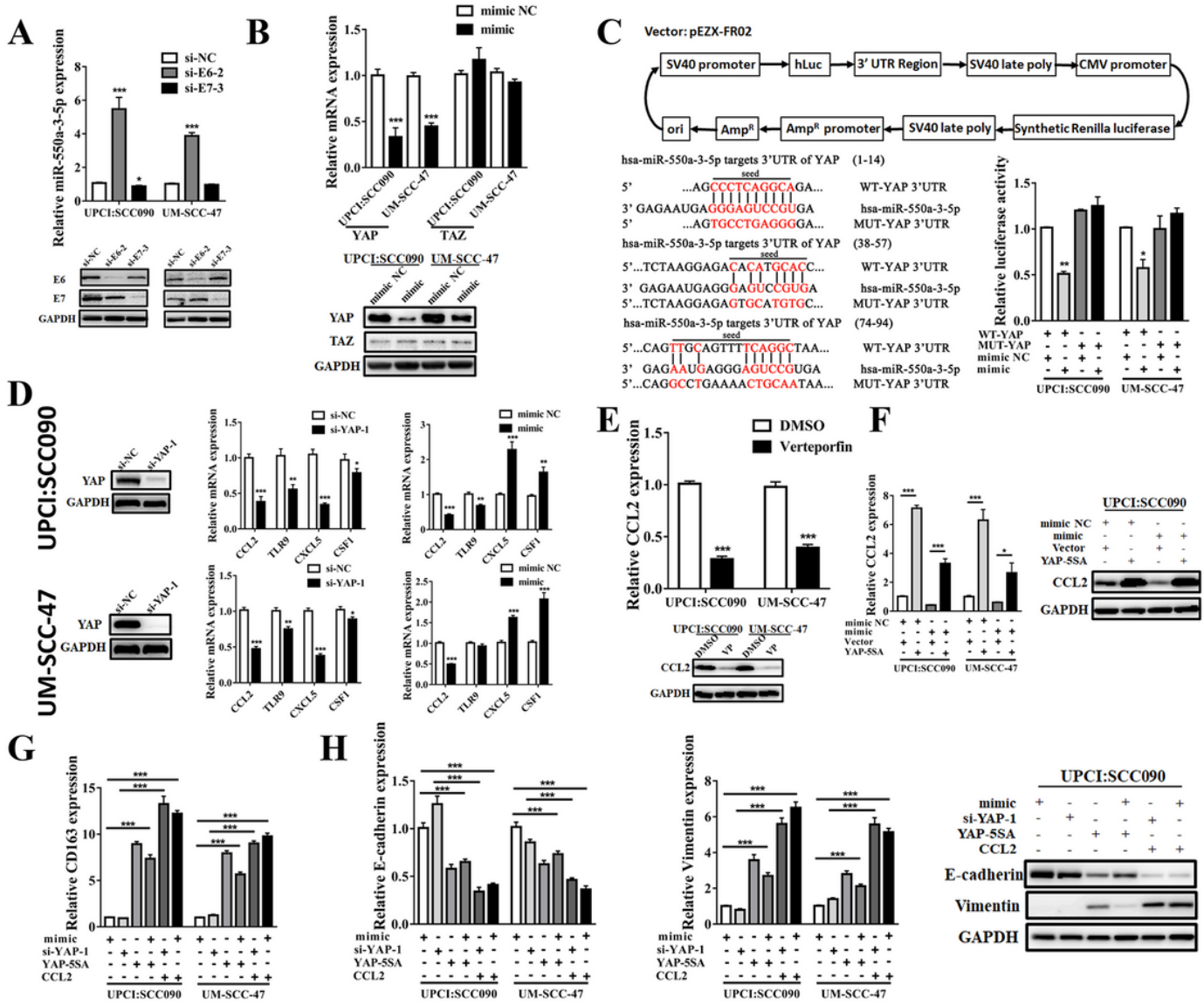

Figure 5

miR-550a-3-5p, down-regulated by E6, inhibited YAP/CCL2 to suppress M2 macrophages polarization and M2 macrophages-induced EMT. (A) Relative expressions of miR-550a-3-5p were examined by qRT-PCR after E6, E7 inhibition in HPV-positive OSCC cells (UPCI:SCC090 and UM-SCC-47). Western blot showed the corresponding protein levels of E6 and E7 after siRNA-mediated knockdown. (B) mRNA and protein levels of YAP and TAZ were examined in miR-550a-3-5p-overexpressed HPV-positive OSCC cells using qRT-PCR and Western blot. (C) Schematic representation of the Vector containing 3'UTR region. Three predicted binding sites for miR-550a-3-5p within YAP 3'UTR wild type (WT) and the mutated sequence (MUT) were indicated in red. Relative activity of luciferase reporters was significantly suppressed in cells co-transfected with WT binding site vectors of YAP 3'UTR in the presence of miR-550a-3-5p mimic. (D) mRNA levels of CCL2, TLR9, CXCL5 and CSF1 were examined in YAP-inhibited and miR-550a-3-5p-overexpressed HPV-positive OSCC cells using qRT-PCR. Western blot was used to detect the protein levels of YAP after siRNA-mediated knockdown. (E) mRNA and protein levels of CCL2 were examined using qRT-

PCR and Western blot in HPV-positive OSCC cells after treatment with verteporfin at a dose of 10 μM for 24 h (DMSO was used as a negative control). (F) mRNA and protein levels of CCL2 were examined using qRT-PCR and Western blot in UPCI:SCC090 and UM-SCC-47 cells co-transfected with miR-550a-3-5p and YAP-5SA. (G) Levels of CD163 were determined by qRT-PCR in PMA-THP-1 cells after exposure to CM from different UPCI:SCC090 and UM-SCC-47 cells for 24 h. Recombinant human CCL2 was added to CM at 500 ng/mL before inducing PMA-THP-1 cells. (H) Levels of E-cadherin and Vimentin were examined by qRT-PCR and Western blot in differentially transfected HPV-positive OSCC cells after co-culturing with their corresponding TAMs for 48 h. All assays were carried out in triplicate. Results were presented as means ± SD. *P 0.05, **P 0.01, ***P 0.001.

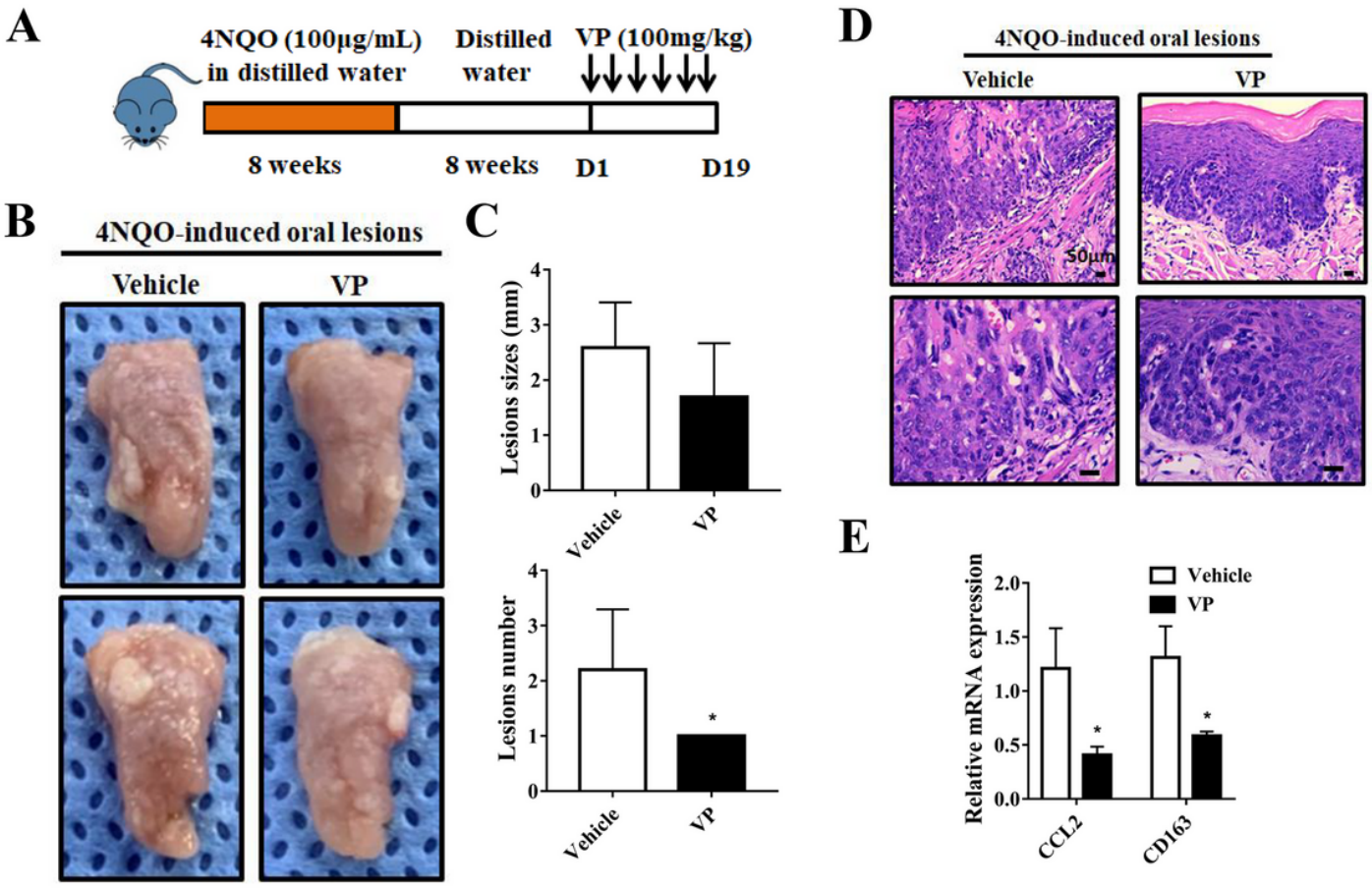

Figure 6

Verteporfin treatment inhibited tumor development in E6-E7 knock-in mice with 4NQO-induced OSCC. (A) Schema of 4NQO-induced OSCC transgenic mice model that were treated with VP (100 mg/kg) at a 3-day interval for 6 doses. (B, C) Representative images of tongue lesions, lesions size and number in Vehicle-treated or VP-treated mice (n=8 per group). (D) Representative images of H&E staining from tumors of Vehicle-treated or VP-treated mice. Scale bars, 50 μm. (E) Expressions of CCL2 and CD163 by qRT-PCR in tumors of Vehicle-treated or VP-treated mice. Quantitative analysis based on triplicate experiments. Results were presented as means ± SD. *P 0.05, **P 0.01, ***P 0.001.

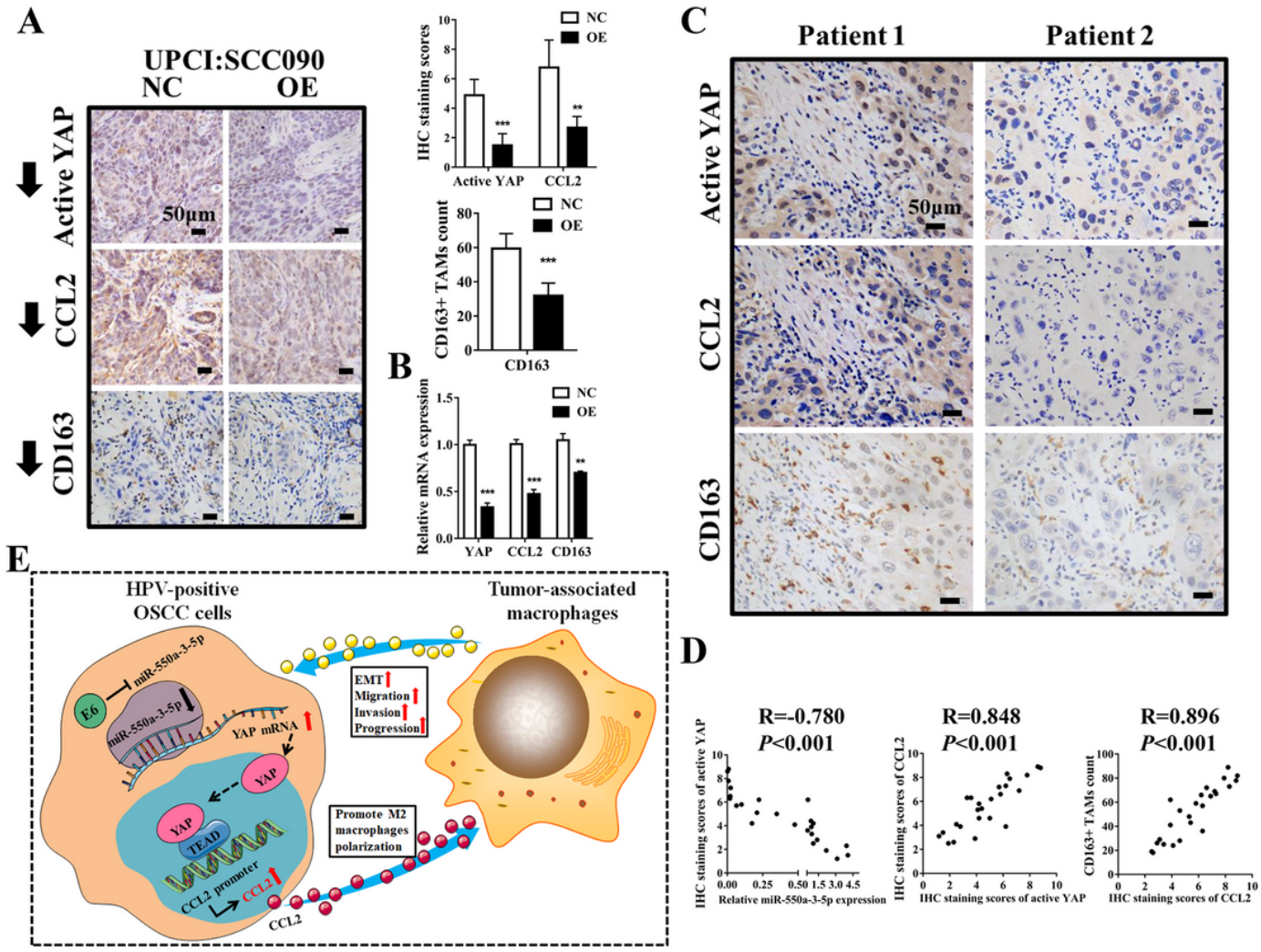

Figure 7

Correlations of miR-550a-3-5p, YAP, CCL2 and M2 macrophages in nude mice xenografts and clinical specimens. (A) Representative images of active YAP, CCL2, and CD163+ M2 macrophages using IHC staining in miR-550a-3-5p-overexpressed UPCI:SCC090 cells-derived nude mice xenografts with quantitative analysis on the right. Scale bars, 50 μm. (B) mRNA levels of YAP, CCL2, and CD163 by qRT-PCR. (C) Levels of active YAP, CCL2, and CD163+ M2 macrophages in representative HPV-positive OSCC patients were shown using IHC staining. Patient 1 had a relatively low expression of miR-550a-3-5p, whereas patient 2 had a relatively high expression of miR-550a-3-5p. Scale bars, 50 μm. (D) Scatterplot depicted a significant inverse correlation between miR-550a-3-5p and YAP, and significant positive correlations between YAP and CCL2, and CCL2 and CD163+ M2 macrophages in cancerous tissues. (E) Proposed model illustrated the role of E6-miR-550a-3-5p-YAP-CCL2-M2 macrophages in regulation of HPV-positive OSCC progression. Quantitative analysis based on triplicate experiments. Results were presented as means ± SD. *P 0.05, **P 0.01, ***P 0.001.

Supplementary Files

This is a list of supplementary files associated with this preprint. Click to download.

- Additionalfile1.tif
- Additionalfile2.tif
- Additionalfile3.tif
- Additionalfile4.docx
- Additionalfile5.docx